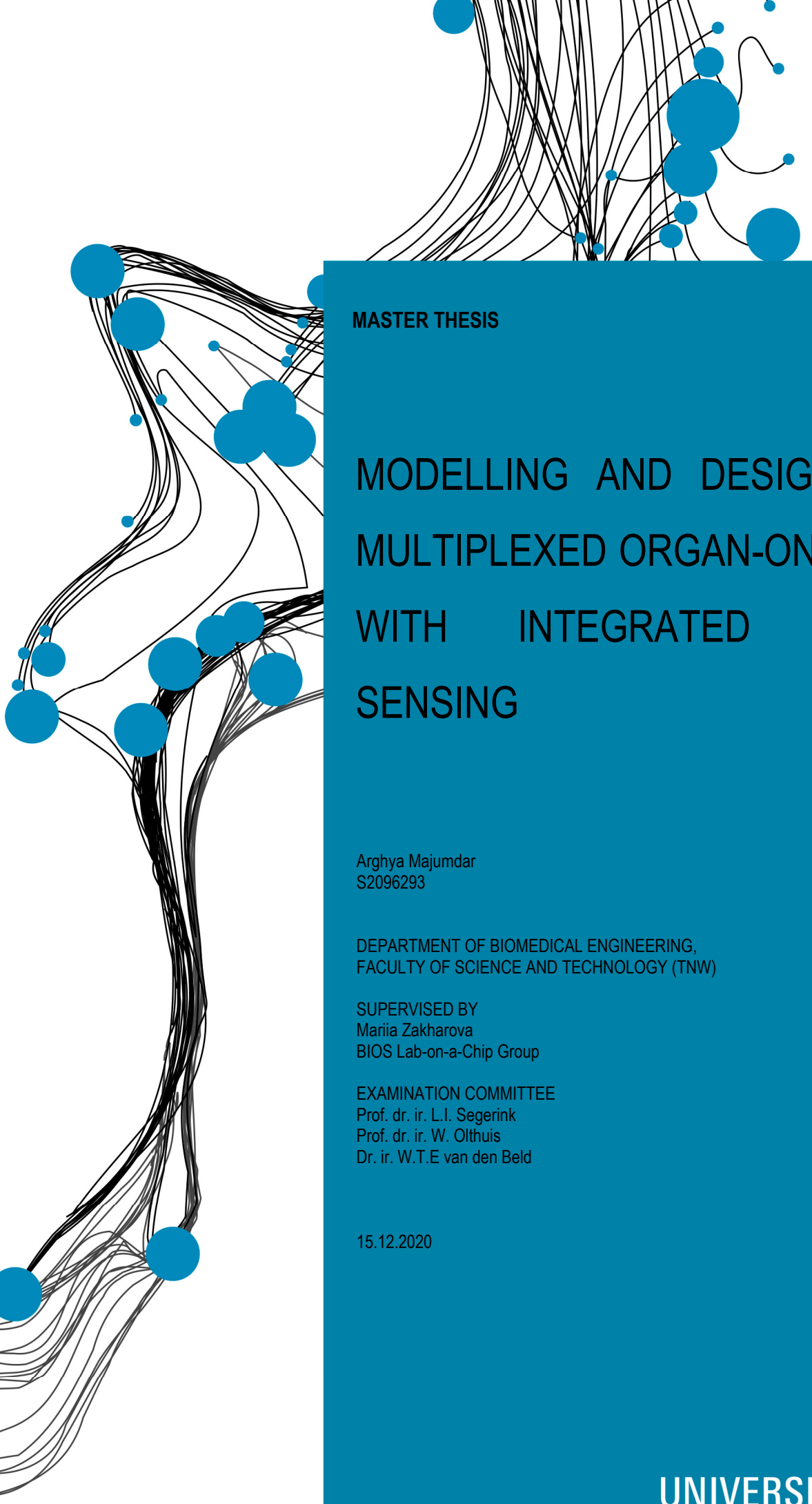

MASTER THESIS

MODELLING AND DESIGN OF MULTIPLEXED ORGAN-ON-CHIP WITH INTEGRATED TEER SENSING

Arghya Majumdar
S2096293

DEPARTMENT OF BIOMEDICAL ENGINEERING,
FACULTY OF SCIENCE AND TECHNOLOGY (TNW)

SUPERVISED BY
Mariia Zakharova
BIOS Lab-on-a-Chip Group

EXAMINATION COMMITTEE
Prof. dr. ir. L.I. Segerink
Prof. dr. ir. W. Olthuis
Dr. ir. W.T.E van den Beld

15.12.2020

UNIVERSITY OF TWENTE.

CONTENTS

ABSTRACT

One of the parameters used in Organ-on-chip platforms to monitor barrier formation and observe the tight junction integrity of the cell cultures is TEER or Transendothelial Electrical Resistance. In this assignment, an Organ-on-chip (OoC) setup was designed with integrated TEER sensing capabilities. The electrode system to be implemented in the chip was modelled and simulation studies were conducted on COMSOL Multiphysics® v5.4. Measurements of TEER in Organ-on-chips often provide erratic results and so sensitivity distribution studies were done to understand the performance of the design. Two different configurations were used to define the electrodes as current-carrying and pick-up electrodes. It was found that in the case of both configurations, the normalized sensitivity (S_n) is less uniform for lower TEER values. However, the distribution approaches uniformity (S_n=1) with an increase in TEER value. The first configuration was found to be less erroneous than the second one, proving the former to be a better option to use. A design of a multiplexed Organ-on-chip was also made on SOLIDWORKS® 2019 with four parallelized channels that have the capability for real-time integrated TEER sensing. Flow simulation was performed to validate the channel geometry used in the design.

ACKNOWLEDGEMENTS

I would like to express my sincere gratitude to my supervisor Mariia Zakharova and co-supervisor Prof. Dr. Ir. Loes Segerink for providing me with the wonderful opportunity to do my Master's thesis assignment with the BIOS Lab-on-a-Chip group of the University of Twente. I would also want to thank them for their constant supervision, guidance and help. I am also grateful towards the other members of the committee, Dr. Ir. Wouter Olthuis of the BIOS-Lab-on-a-chip Group and Dr. Ir. Wesley van den Beld of the XUV Optics group for finding out time from their busy schedule to be a part of the assessment. I have been able to learn a lot from this challenging experience and hopefully, it will help me grow as an individual both professionally and personally.

Last but not the least, I am forever thankful to my parents, Ananda and Jayati, and my elder brother, Ayan for their constant support and encouragement.

LIST OF ABBREVIATIONS

AC- Alternating Current

ALI- Acute Lung Injury

BBB- Blood Brain Barrier

BBBoC- Blood-Brain-Barrier-on-chip

BMEC- Brain Microvascular Endothelial Cell

BoC- Brain-on-chip

CC- Current Carrying

CNS- Central Nervous System

DC- Direct Current

EVOM- Epithelial Voltohmmeter

HUVEC- Human Umbilical Vein Endothelial Cell

NVU- Neurovascular Unit

OoC- Organ-on-chip

PC- Polycarbonate

PDMS- Polydimethylsiloxane

PET- Polyethylene terephthalate

PU- Pick Up

TEER- Transendothelial Electrical Resistance

1 THE BLOOD BRAIN BARRIER

The Blood Brain Barrier (BBB) is a highly selective semi-permeable membrane that keeps the blood circulating through the blood vessels separated from the brain and extracellular fluid in the central nervous system (CNS) [1]. It allows the passive diffusion of selective molecules (O_2, CO_2, hormones) and enables the transport of glucose, water and amino acids that are critical for the functioning of the neuronal system [2-3]. It blocks large (> 400 Da) and potentially toxic molecules from passing into the brain [4]. The BBB protects the brain from harmful foreign substances in the blood, from hormones and neurotransmitters present in the rest of the body and maintains a stable environment for the brain. As the tight junctions of the BBB keep bacteria out of the brain, they also prevent the entry of antibodies and antibiotics. This causes treatment of brain infections very difficult [5]. Cancer cells in the brain are also quite difficult to treat with chemotherapeutics, which are not normally allowed to pass into the brain by the BBB and are often transported out of cells by multidrug transporters.

The high selectivity of the barrier, thus, makes it very difficult to determine which drugs will be allowed by the barrier to pass through. This makes neurodegenerative drug delivery very complicated and thereby has hindered the possibility of finding a cure for diseases such as Alzheimer's disease, Parkinson's disease, multiple sclerosis etc. [5].

The BBB is formed by the tight junctions between brain endothelial cells which comprise of subunits of transmembrane proteins, such as occludin, claudins etc. The proteins are attached to the endothelial cells by a protein complex that includes tight junction protein 1 and associated proteins [6]. The other components that make up the blood-brain barrier other than the endothelial cells are pericytes, astrocyte end-feet, microglia and basement membrane made from structural proteins such as collagen and laminin. Figure 1 provides the structural outline of the BBB. The BBB also contains Aquaporins (water channels) which enable the transport of water across the blood-brain barrier.

The ease of transport of a certain molecule (including drugs) through the BBB is dependent on multiple factors such as [7]:

- **Lipid solubility** of compounds. The compounds which are more lipid soluble cross the barrier with more ease.
- **Charge at physiological pH:** Molecules which have a higher charge at physiological pH (7.4) is more commonly blocked by the barrier.
- **Presence of efflux transporters** may prevent the distribution of the drug inside the CNS and instead excrete the drug back to the bloodstream.
- **Co-dependency of protein binding** in the molecules. Higher the presence of protein binding co-dependency, lower are the chances of passage through the BBB.

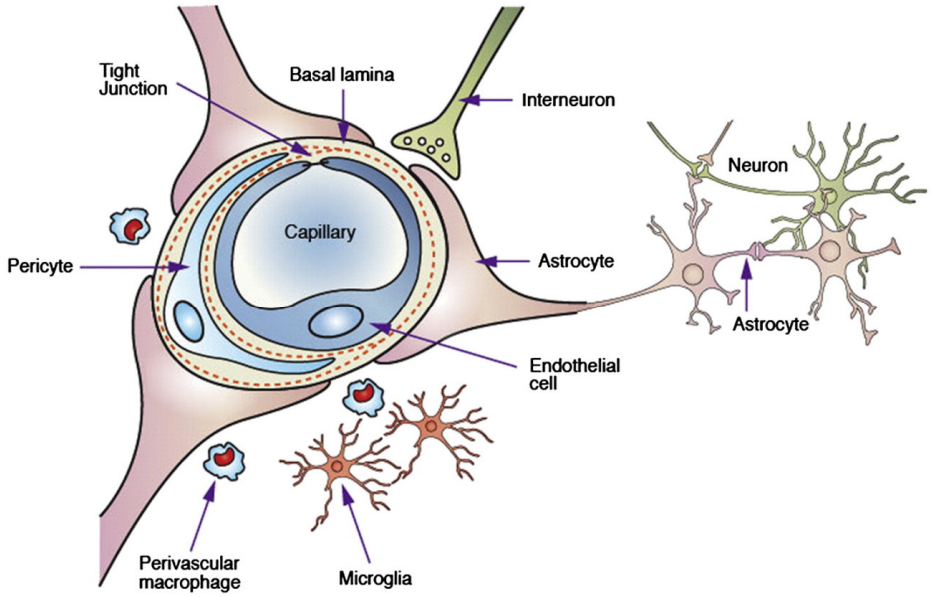

Figure 1: ***The Structure of the Blood Brain Barrier****: The barrier mainly constitutes of endothelial cells, astrocyte end-feet and pericytes. The endothelial cells act as barriers around the blood vessels of the brain. The pericytes help in regulating peripheral blood flow and the permeability of the barrier by signalling to neurons, endothelial cells and astrocytes. The astrocytes of the BBB maintain signal communication between the endothelial cells and the pericytes. Image is adapted from Chen et al. [7]*

The BBB is highly selective which, in terms of drug transport, means only specific drug molecules can pass through the barrier which fulfils one of the criteria below:

- The molecules have high partition coefficients, are highly lipid soluble. This allows them to diffuse through the barrier easily passively. These molecules gain entrance quicker.
- The molecules are moderately lipid soluble and are possess partial ionisation. These molecules gain access through the barrier slower.

A molecule, if permitted to pass, is transported through the BBB via various mechanisms depending on the molecule's chemical nature. The mechanisms are namely Paracellular Transport, Transcellular Transport, Transport Proteins, Efflux Pumps, Receptor-mediated Transcytosis, Absorptive Transcytosis and Cell-mediated Transcytosis. (See Figure 2 for a schematic representation of these mechanisms.)

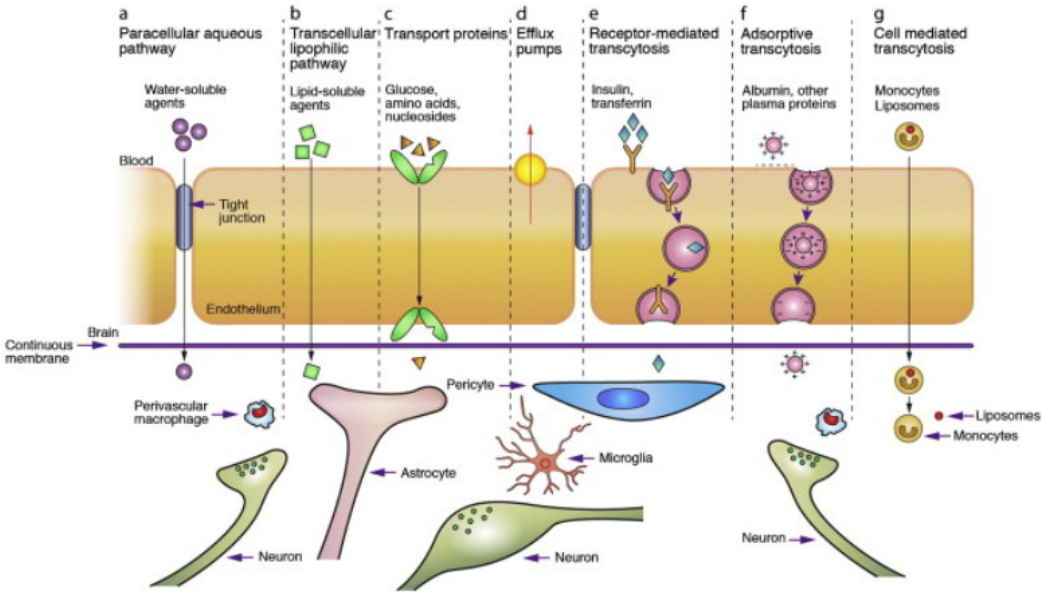

Figure 2*: **A Schematic Representation of Transport Mechanisms of the BBB:** The figure shows the various mechanisms involved in molecular transport through the BBB such as Paracellular Transport, Transcellular Transport, Transport Protein mediated delivery, Efflux Pump, Receptor-mediated Transcytosis, Absorptive Transcytosis and Cell-mediated Transcytosis. The most investigated targeting route of the BBB transport is receptor-mediated transcytosis and it is believed that nanoparticles are transported by this mechanism. Image adapted from Chen et al. [7]*

A proper understanding of the structural and functional characteristics and the various transport mechanisms involved within the BBB is necessary to find out a method to optimally deliver drugs inside the brain and thereby treat neurodegenerative diseases.

Drugs are usually tested on animal subjects for screening but they do not necessarily have the same effect as it would have on a human subject. This led to the urgency of developing alternative platforms to aid in drug screening, with Organ-on-chip being one such platform that can mimic the organ level function of humans on a microfluidic platform.

2 THE ORGAN-ON-CHIP PLATFORM

Presently, most of the drug testing is carried out in animals such as rats, mouse etc. Though they provide a good insight into the effectiveness of the drug, they often do not translate well in humans [8]. This served as a motivation to find alternative platforms for drug testing and drug screening. The growing research and development of microfluidic platforms have led to the advent of one such alternative: microfluidics-based Organ-on-chip (OoC) devices [9].

A microfluidic platform is designed to manipulate the flow of fluids of volumes ranging from picolitres (10^{-12}) to microlitres (10^{-6}) in a channel network for different applications. The exponential growth of popularity of the platform since the 1990s has led to the progress of biomedical research as well [9]**.** Organ-on-chips are an application of this platform which are designed to mimic the physiological functions of various organs and tissue barriers [10]. These chips usually have an organised cell culture on a porous membrane that is grown with continuous perfusion of fresh medium inside a channel on the chip. Depending on the purpose, the cell culture may be a simple monoculture or a more complex co-culture of cells. The co-culture is often preferred to study tissue barriers such as the Blood-Brain Barrier (BBB).

The devices can mimic conditions when a certain disease or some other physiological condition occurs (e.g., hypoxia). This aids in the study of these conditions and has made OoCs a very important tool for drug screening and testing [11].

The development of the platform kickstarted when *Rohr et al.* [11] published his study in 1991, which, was the first such occurrence of using organized cell culture to study diseases. The purpose of the work was to study ventricular myocardium *in-vitro*. This, along with the introduction of Polydimethylsiloxane (PDMS), led to the massive growth of bio-microfluidics [12]. PDMS has some unique physical, chemical and fluidic properties which were found to be extremely suitable for small scale bio-applications. The first proper breakthrough of OoC development came in 2004. *Michael Shuler et al.* [13] managed to mimic human physiology at an organ-level using cell culture within a microfluidic chip. It managed to show the systematic interaction between liver and lungs on one square-inch silicon-based chip. Since then, a wide range of human organs has been mimicked in a microfluidic platform.

2.1) The Development of Blood-Brain Barrier-on-a-Chip

The progressive degeneration of neurons leads to neurodegenerative diseases that have no therapeutic cure as of now. Currently, there is a list of FDA approved drugs which can only reduce the symptoms. Many studies are being conducted regarding the concerned drugs, to figure out the most effective one. As a result, an efficient drug screening platform is highly desirable.

In-vitro BBB models are being widely used as one such platform. The studies based on *in-vitro* models put a lot of importance on the development of microfluidic chip systems which can mimic the organ level functionality of human physiology. One of the most widely used methods is the implementation of Transwell® systems. The system incorporates a BBB tight junction by culturing monolayer of endothelial cells on the apical side and neuronal cells on the basolateral side of the plate. Depending on the complexity of the junction desired, the neuronal cell culture may consist of only astrocytes or a co-culture of astrocytes, pericytes etc. *Borges et al.* [14] and *Hartz et al.* [15] developed a single cell Transwell® system consisting of a cultured monolayer of Human Umbilical Vein Endothelial Cells (HUVECs). These systems, although were simple, provided important information regarding the physiological behaviour of the cells. *Wang et al.* [16] co-cultured Brain Microvascular Endothelial Cells (BMECs) and astrocytes on the apical and basolateral sides of the microwell plates respectively. The model required less experimentation time and as well as proved to be cost-effective. The culture also displayed stability of the tight junctions.

Recently, organ-on-chips have become a popular field of research and development. *Bang et al.* [17] established a novel three-dimensional Neurovascular-Unit-on-chip. The chip contained a co-culture of astrocytes and neurons to establish a vascular network. Two separate channels were designed to allow flow of two different media. This allowed mimicking highly localized internal as well as external microenvironments.

Yeon et al. [18] published a study about a PDMS device that contains two channels of 25µm height which are connected by microholes. Different flow rates were applied in the channels and the pressure differential generated in these microholes trapped the HUVECs hydrodynamically inside and near each other. The tight junction formation occurred after a period of incubation (23 hours). Different drugs were introduced at the side of the microholes away from the cells. The permeability of the drugs through the barrier was assessed with fluorescence microscopy and high-performance liquid chromatography.

Terrell-Hall et al. [19] developed a four-channel OoC system that contained two central gel regions for co-culturing astrocytes and neurons. The gel region was surrounded by two side channels as outer compartment which contained the endothelial cells and cell medium. In between the central and the surrounding outer parts, there were pores of 3µm diameter which allowed diffusion of media and tracers which is necessary for performing kinetic studies of solute molecules in the media. The chip was used for the study of permeability across an in-vitro blood-tumour barrier.

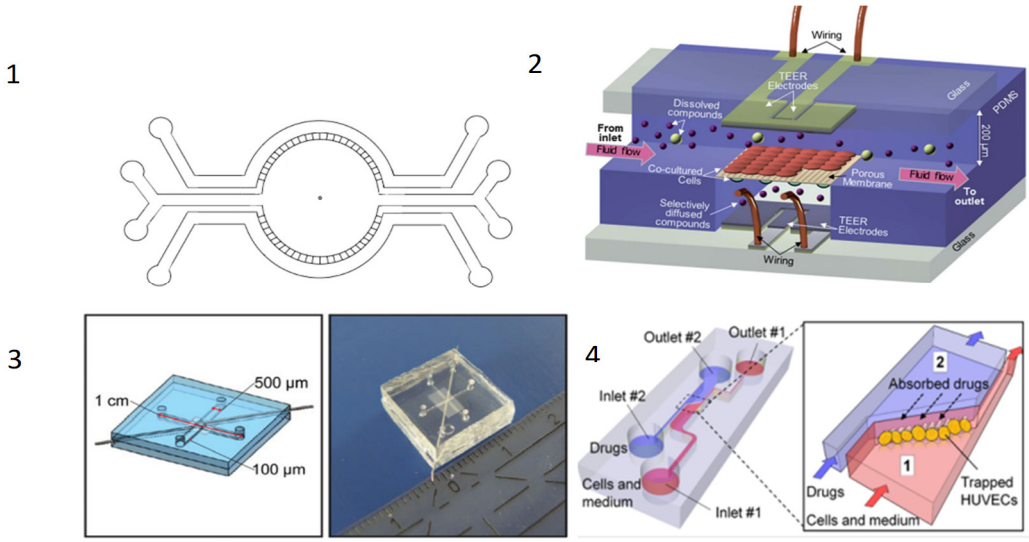

Figure 3: ***Various BBB-on-Chip devices developed:*** *The figure shows the different BBB-on-chip platforms that have been developed over the years. (1) The 2D top view of the chip channel design by Terrell-Hall et al. [19], (2) The "µBBB" with integrated glass electrodes to facilitate TEER measurements on-chip (Adapted from Booth et al. [20]), (3) The two-layered PDMS chip by Griep et al. [21] which had Pt wire electrodes inserted into the top and bottom channel grooves of the chip and correctly positioned to measure TEER of the cell culture on a small membrane. (4) The BBB-on-chip system consists of microholes which hydrodynamically trap HUVECs which form the barrier after a period of incubation. Drugs, whose permeability are to be measured, are introduced through the side of the microholes not containing the cells (Image adapted from Yeon et al. [18].*

Booth et al. [20] made a Blood-Brain-Barrier-on-chip (BBBoC), called the µBBB, with semi-transparent glass electrodes fabricated in the chip to facilitate Transendothelial Electrical Resistance (TEER) measurements. It was a dual-layer BBB culture comprising of endothelial cells and astrocytes. The chip comprised of a polycarbonate (PC) membrane on which the cells were cultured, sandwiched between two PDMS channel layers for flow of media. The design also implemented high-density electrodes with 200mm gaps between each electrode for measurement of TEER. The transparency of the substrate and the design and positioning of the electrodes also provided windows to perform microscopy. The model had a small functional volume, required relatively less time to achieve steady-state TEER values- decreased turn-around, and provided a chance for an increased high-throughput approach to experimentation.

A two-layered PDMS based BBB chip was developed by *Griep et al.* [21] with a membrane separating the top and bottom layer. The chip had a culture area 4 times smaller than the one required by *Booth et al.* [20]. This drastically reduced the number of cells required to be seeded for the experiments and in turn reduced the amount of media and drugs required to be perfused. The device incorporated inert Pt wire electrodes in place of widely used Ag/AgCl electrodes which are oxidation sensitive and thereby improving the reliability of the electrical TEER measurements for judging the tightness of the BBB junctions. The Pt wire electrodes were slid into the top and bottom groves and held in position by a special adhesive.

Van der Helm et al. [22] made a similar multilayer OoC as *Griep et al* [21] with certain modifications such as the positioning of the electrodes. Unlike before, wire electrodes of 200um diameter were inserted at each end of both top and bottom channels, i.e., a total of four electrodes were used (two on top and two on bottom). The electrodes were inserted carefully so that their ends were positioned directly on the top and bottom of the culture.

Figure 3 provides an overview of the different OoC platforms.

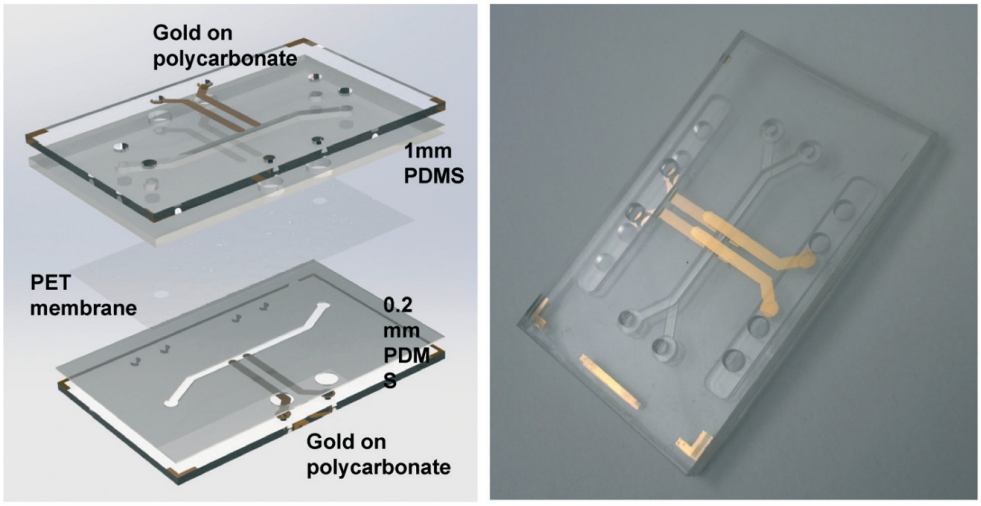

Figure 4: ***Organ-on-chip design with integrated gold electrodes by Henry et al. [18]:*** *Semi-transparent gold electrodes were patterned on a polycarbonate (PC) layer. The chip comprised of two PDMS channel layers with a PET membrane sandwiched in between them. The PC layers with the patterned electrodes were placed as the top-most and bottom-most layers of the chip.*

Henry et al. [23] fabricated a chip with integrated gold electrodes patterned on a polycarbonate layer which would allow measuring TEER directly from the chip (Figure 4). The chip was assembled by aligning a thin porous Polyethylene terephthalate (PET) membrane with a thin PC/PDMS (0.2mm) layer which represented the basal microfluidic compartment of the OoC and covered them with a thicker PC/PDMS (1mm) layer that represented the apical compartment. The fabricated electrodes were semi-transparent and the system allowed measurement of both the TEER and cell layer capacitance of the cell culture. A 4-point impedance measurement was done over a frequency spectrum of 10Hz to 1MHz. From the TEER measurements, the researchers could differentiate between human primary small airway epithelial cells under acute lung injury (ALI) culture conditions and human intestinal epithelial cells covered by flowing medium on-chip. The chip could also indicate the disruption of cell–cell junctions from the drop in TEER levels upon exposure to the chelating agent EGTA.

Maoz et al. [24] developed a Neurovascular Unit-on-a-chip system which comprised of three chips: two BBB-on-a-chips (BBB $Chip_{in}$ and $BBBChip_{out}$) and a Brain-on-a-chip (BoC). In the BBB chips, a continuous monolayer of primary human brain endothelial cells was cultured on the lower surface of a PET

membrane and a co-culture of astrocytes and pericytes was developed on the upper surface of the membrane.

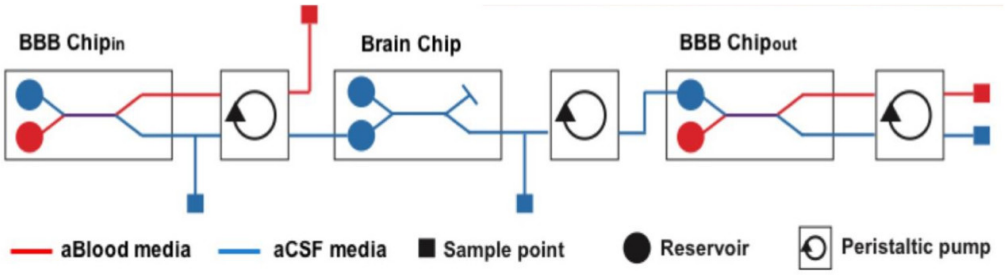

Figure 5: ***NVU flow as obtained by Maoz et al. [24]:*** *The BBB-influx chip, Brain chip and the BBB-efflux chip are connected by silicon tubes. the media is pumped from the outlet of one chip to the inlet of the other (from the BBB Chip$_{in}$ → Brain chip → BBB Chip$_{out}$) via peristaltic pumps. The channel for the flow of artificial CSF is marked in blue and that of artificial blood is marked in red.*

Each of the three chips consisted of three layers: an upper PDMS channel layer, a porous PET membrane in the middle and a lower PDMS channel layer. The top channel of the BBB chip served as the perivascular compartment of the BBB while the bottom channel mimicked the flow for the vascular portion of the BBB. The cell culture on the membrane represented the tight cellular junction of the BBB. The three chips were connected via proper tubing and a continuous flow of media through the chips was ensured by using peristaltic pumps (Figure 5). Samples of the flow media were taken out at the outlets of each chip to measure the concentration of drugs in each. A comparison of the concentrations was done to understand which one crossed the tight junction more effectively.

The development of PDMS has led to an increase in research based on the microfluidic platform and especially OoCs [9]. This has led to researchers experimenting with different designs and setups to mimic the BBB on a chip. The microfluidic platform allows for easier manipulation of the flow of the media which aids in studying the BBB culture in a dynamic environment. This is an immediate advantage over the conventional Transwell® models. Additionally, the OoCs have provisions to integrate electrode systems directly on the chip which allows for direct TEER measurements of the cultures. Integrated electrodes do away with the problem of manual handling of STX-2/chopstick electrodes that are generally used with Transwell® models. This thereby reduces the errors in measurement that may happen due to shaking of hands altering the position of the electrodes during measurements. However, this does not reduce the complexity and erraticism of TEER measurements since the measurement sensitivity is highly dependent on the geometry of both the electrodes and the channels of the chip. It also depends on the electrode positions, the method of excitation used etc. These are further discussed in the later chapters.

These have motivated studies to be done to figure out a way to reduce the variation of TEER measurements from system-to-system, of which, sensitivity studies are of particular importance.

2.2) TEER Measurement in Organ-on-Chips

TEER or Transendothelial Electrical Resistance is the electrical resistance across a cellular monolayer which is highly sensitive to the integrity and permeability of the monolayer [25]. This made TEER a popular choice to check the tissue barrier integrity and tightness. Electrodes are used to pick up voltage readings from applied current excitations to measure the TEER of cell cultures, the methods of which are discussed in further details in **chapter 3**. The main advantage of the use of electrode systems is that it allowed real-time TEER analysis which is important in monitoring the tight junction integrity under dynamic conditions.

However, a fixed standard measurement of TEER for a particular type of culture is yet to be established. This is because of the high dependency of the value on factors like the culture area, dimensions of the media channels, position and dimension of electrodes used as well as the proximity of the excitation and readout electrodes [26-27]. One more important factor is the distance between the electrodes and the cell culture. That is why a normalization study of the current sensitivity of electrodes is done to understand the TEER measurement accuracy of the device.

To understand how the geometry of an OoC affects the measured TEER, *Yeste et al.* [26-27] made a COMSOL Multiphysics® simulation study of a simple chip design where they used three different channel heights (100um, 200um and 500um) as well four different electrode setups to check the normalized current sensitivity (Figure 6). Ideally, the normalized current sensitivity should be 1 and be fixed for all TEER values but this is quite difficult to achieve practically. The study by *Yeste et al.* [27] found that the best result was obtained when the distance between the centres of the readout and current-carrying electrodes is close to the chamber height. TEER dependency on the sensitivity was found in all the models and it was found that higher the TEER, more uniform is the sensitivity distribution.

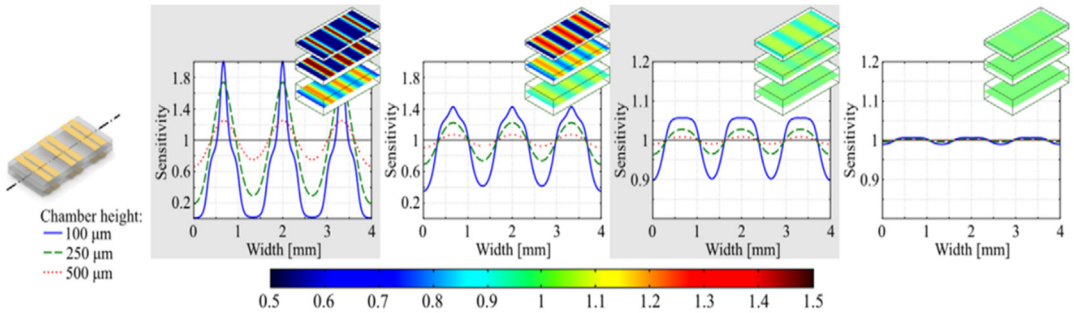

Figure 6: ***Normalized Current Sensitivity results obtained by Yeste et al. [27]:*** *Sensitivity distribution along the cell layer through the axis (dash-dotted line) shown in the 3D model on the left when TEER is measured in the microfluidic. Results are presented for different TEERs (100, 10^1, 10^2, 10^3 Ω*cm^2) and different channel heights (100, 250 and 500 µm). Data normalisation was done by multiplying the actual Current Sensitivity with the square of the cell culture area.*

A numerical analysis study performed by *van der Helm et al.* [22] measured TEER of cell culture of a Gut-on-chip. A channel height of 1mm was used with 1mm wide

electrodes. The centres of the readout and excitation electrodes were placed 1mm apart. In their results, the effect of the TEER value on the sensitivity was quite high but it also showed that for higher TEER the sensitivity is more uniform and closer to 1.

2.3) Organ-on-Chip Multiplexing

Organ-on-chips are primarily used for drug testing and screening. This often involves a large number of drugs and hence testing them on a single cell-cultured chip would lead to a long experiment time and a tedious process. This led to the demand for multiplexed Organ-on-chips so that multiple drugs can be tested parallelly.

There are a lot of challenges when it comes to multiplexing of different chips. Often, to facilitate simultaneous flow to all the channels, a common inlet is designed. The problem that arises in these cases is the even distribution of the media flow and pressure amongst all the channels. There are also risks of crosstalk between two adjacent channels which may affect the condition within each channel. So, while designing a multiplexed chip, the possibility of contamination due to diffusion and advection of solutes into adjacent channels must be considered [28]. To tackle this problem, choosing proper channel dimensions and branching are required.

An example of a multiplexed OoC design is the device published by *Zakharova et al.* [28]. The multiplexed chip has eight parallel channels (500µm × 50µm). All the channels branch out from a common inlet and consist of separate access ports. The incorporation of the common inlet facilitates the simultaneous filling of all the channels (Figure 7).

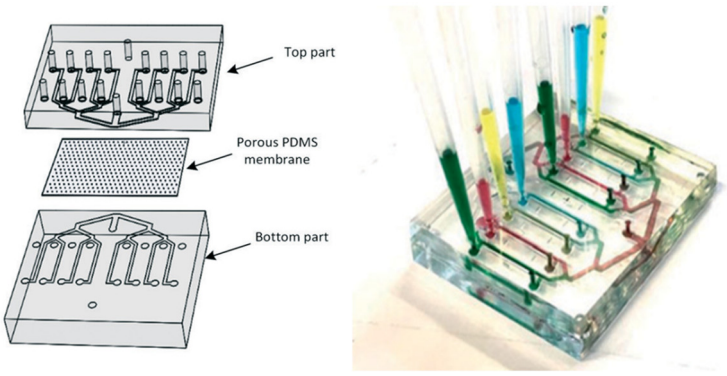

Figure 7: ***Multiplexed Organ-on-chip design proposed by Zakharova et al. [28]:*** *The design comprises of 8 channels (on top and bottom) branching off from a common inlet. Each of the channels has its outlets which can be used to perform up to 8 separate experiments simultaneously as shown on the right side of the figure. The left of the figure shows the different parts of the design.*

The placement of the inlet was done such that it is at the same distance from each of the branching channels to ensure an even distribution of the flow and cells through the channels. The channels are however provided with their outlets. This was done to make each channel accessible to perform eight separate experimental conditions simultaneously.

Another aim of Organ-on-chip multiplexing is to integrate different types of Organ-on-chips to build towards a Human-on-chip. This proves to be quite complicated since it leads to scaling and vascularization issues [29]. Each 'organ' that are being multiplexed must have the *in-vivo* scale ratios translated properly *in-vitro* to facilitate proper functionality and this depends highly on the type of organs being multiplexed. The limitations highlight the need to find scaling methods using engineering concepts or by simulating different mathematical or computer models to reduce errors before experimentally working on a setup.

3 TEER MEASUREMENT TECHNIQUES

Transendothelial Electrical Resistance or TEER is one of the most accepted methods for measuring tight junction integrity and cell physiological conditions in cell culture models *in-vitro* [30]. The ability of TEER to indicate the conditions of cellular barriers aids in effective drug transport studies.

One of the main advantages of the technique is that it can provide real-time measurements without damaging cells, thereby helping in active monitoring the cellular barrier dynamics while an agent is being supplied to the flow media to have it transported across the barrier [30].

The TEER measurement can be done in mainly two ways, by measuring ohmic resistance or by measuring the impedance over a wide range of frequencies. The technique of measuring TEER is already used in Transwell® systems using chopstick electrodes. TEER measurement is also used in case of OoCs by integrating electrodes into the chip.

3.1) Ohm's Law Method

By this method, the cellular barrier integrity is measured by calculating the resistance of the cellular layer. An electrode pair is used for this purpose. One of the electrodes is positioned in the apical compartment, and the other in the basolateral compartment (see Figure 8). The two sides are separated by the cell layer whose TEER is required to be obtained.

The resistance of the cell layer is calculated by providing a direct current (DC) voltage to the electrodes and measuring the resulting current. The resistance is calculated using Ohm's Law: the ratio of the voltage applied to the electrodes and the current produced. A downside of using DC currents is that if the excitation is too high or prolonged it can cause damage to the cells by irreversibly destroying the cell membranes. This can be controlled by applying a square alternating current (AC) voltage waveform as input signal instead.

A lot of commercially available devices are present that can be used for ohmic resistance measurement. One of the popular devices is Epithelial Voltohmmeter (EVOM). It provides a square Alternating Current waveform at a frequency of about 12.5Hz [30]. This prevents the chances of charging effects on the electrodes and the cell layer, thereby preventing any damage to the cells and the electrodes. To measure the resistance, a pair of chopstick electrodes (STX2) is used.

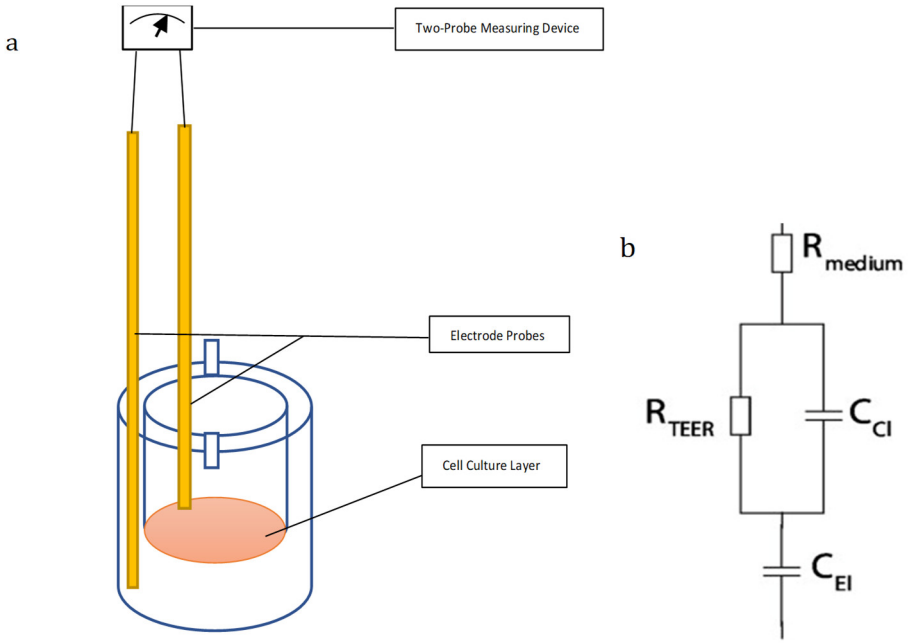

Figure 8: ***The Standard Setup for Ohmic Resistance Measurement Method:*** (a) *A cellular monolayer cultured on a semipermeable insert serves as the divide between the apical and basolateral compartments. Two STX2/chopstick electrodes are inserted, one on each side with the monolayer in between them. Voltage is applied to the electrodes and the current produced is measured by the same pair. The two values are then used to measure the resistance using Ohm's Law. (b) The total electrical resistance includes the resistance of the cell layer* R_{TEER}*, the cell culture medium* R_M*, the semipermeable membrane* R_I *and the electrode medium interface* R_{EMI}*. (Image adapted from Benson et al. [32]).*

The measurement procedure first involves reading the blank resistance of the membrane which does not have any cells cultured on it (R_{BLANK}), followed by measuring the resistance of the cell monolayer on the membrane (R_{CELLS}). The cell resistance (R_{TISSUE}) can be calculated from the equation below:

$$R_{TISSUE}(\Omega) = R_{CELLS}(\Omega) - R_{BLANK}(\Omega) \quad (1)$$

The calculated R_{TISSUE} is the resistance of only the cell monolayer since R_{CELLS} contains the resistance of both the cell layer and the membrane and that is the reason deducting the value R_{BLANK} is necessary for accurate measurements. TEER is calculated from R_{TISSUE} by:

$$TEER_{measured}(\Omega.cm^2) = R_{TISSUE}(\Omega) \times M_{area}\,(cm^2) \quad (2)$$

Here, M_{area} is the effective area of the membrane used for the culture.

3.2) Impedance Spectroscopy Method

Impedance Spectroscopy is a more reliable method for calculating TEER than Ohm's Law Method. The accuracy of measurement which depends on the measuring algorithm used for the quantification [31]. A small amplitude AC signal having a frequency sweep (usually ranging from 10Hz to 10MHz) is provided and

the amplitude and phase response analysis of the current generated in the monolayer is done. The impedance (Z) is defined as the ratio of the voltage-time function (V(t)) and the current-time function (I(t)):

$$Z(\Omega) = \frac{V(t)}{I(t)} = \frac{V_0 \sin(2\pi f t)}{I_0 \sin(2\pi f t + \phi)} \tag{3}$$

In equation (3), V_0 and I_0 are the peak voltage and current in Volts and Ampere respectively, f is the frequency of the applied signal in Hz, t is the time in seconds, φ is the phase shift between the voltage-time and current-time functions in degrees. The impedance (Z) is a complex function and can be represented by its magnitude |Z| and the phase shift or as the sum of its real part (Z_R) and the imaginary part (Z_I).

The measured impedance can be represented in terms of the magnitude and phase as:

$$Z(\Omega) = |Z|e^{j\phi} \tag{4}$$

The exponential part of the equation (4) provides the frequency spectrum of the impedance. The advantage of this technique is that by measuring impedance over a wide range of frequency, one can get additional information regarding the cell capacitance which cannot be obtained by using the Ohm's law method. A commercially available automated system such as cellZscope® (nanoAnalytics GmbH, Germany) can measure the transendothelial impedance of cell layers on permeable membranes. In this method an equivalent electrical circuit analysis of the measured impedance spectrum is done which is then used to characterize the cellular barrier properties [32].

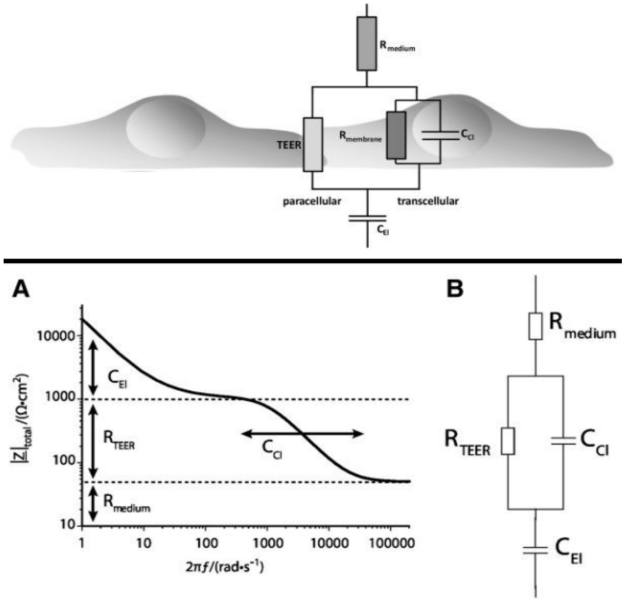

Figure 9: ***Impedance Spectroscopy Method:*** *(Top) Electrical Equivalent Circuit used to analyse the Impedance Spectrum of biological cells, (Bottom) a) Impedance Spectrum with different frequency dependent regions, b) Simplified Electrical Circuit Model. Adapted from the work done by Benson et al. [32]*

The electrical equivalent circuit model is shown in Figure 9. On providing an excitation, the generated current can flow either through the junction between the cells (paracellular route) or through the cell membrane (transcellular route). The tight junction proteins present in the paracellular route results in the resistance (R_{TEER}). The lipid bilayers present in the transcellular route generate a parallel circuit comprising of a parallel combination of resistance ($R_{membrane}$) and electrical capacitance (C_{Cl}) [32]. The resistance of the cell culture medium (R_{medium}) and the capacitance of the measurement electrodes (C_{El}) also contribute to the model. The value of $R_{membrane}$ is high and this forces most of the current to flow through the capacitive path. This allows an approximation where $R_{membrane}$ can be neglected and the lipid bilayers can be solely represented by the capacitive element.

Thus, the equivalent circuit diagram can be further simplified as shown in part (b) of the bottom picture of Figure 9 and the impedance spectrum observed have a non-linear frequency dependency as shown in part (a) of Figure 9.

The impedance spectrum of a cell comprises of three distinct frequency regions. In each of these regions, the cell impedance is dominantly influenced by a particular element of the equivalent circuit. In the low-frequency range (<10Hz), the impedance provides information regarding the capacitance developed due to the electrode-electrolyte double layer (C_{El}). In the middle frequency range (10Hz to 10MHz), the impedance signal provides information of both the TEER of the cell layer (R_{TEER}) as well as the cell layer capacitance (C_{Cl}). In the region of high frequency (>10MHz), the circuit capacitance C_{Cl} and C_{El} provide a more conductive path and the impedance signal is dominated by the element R_{medium}. These parameter estimations can be obtained by performing fitting of the experimental impedance spectrum data to the equivalent circuit model by applying non-linear least-squares fitting.

3.3) Electrode Sensing Method for Resistivity Measurements

At the core of measuring TEER via impedance measurements is the process of measuring the resistivity or conductivity of the cell culture. There are two probable ways of doing so:

- Two-probe Method
- Four-probe Method

3.3.1) Two-Probe Method

In two-probe device, a small amount of voltage is applied to the material of interest (in this context it is the cell culture) via a pair of electrodes. The current flowing across the two contact points of the electrodes is measured which gives the resistance value (following Ohm's law). Although at first sight, this measurement technique seems ideal, a major problem of the method is that the same electrode pair is being utilized for providing the test voltage and for sensing the current

generated due to the excitation [33]. This leads to the internal resistance of the electrode probes getting added to the actual measurement. Thus, an inaccurate measurement is obtained which could prove vital in certain applications and especially when dealing with bio-applications.

In the case of this sort of measurement, STX2 electrodes/EVOM2 setup is usually used in the method discussed under **section 3.1**. The additional problem using them is that the electrodes are usually positioned in a Transwell based bioreactor by hand. The readings obtained from EVOM2 are highly dependent on the positioning of the electrodes and, thus, requires careful handling of the probes when they are introduced into the Transwell to prevent any disturbance.

The uniformity of current density, generated by the electrodes, also affect the TEER measurements significantly. For example, the STX2/chopstick electrode is not capable of providing a uniform current density over a large membrane, such as the 24mm diameter tissue culture inserts, and this leads to an overestimation of the TEER value [34].

The problems of this method led to the increasing implementation of a more improved method called the "Four-probe Method" or "Four Terminal (4T) Method".

3.3.2) Four-Probe Method

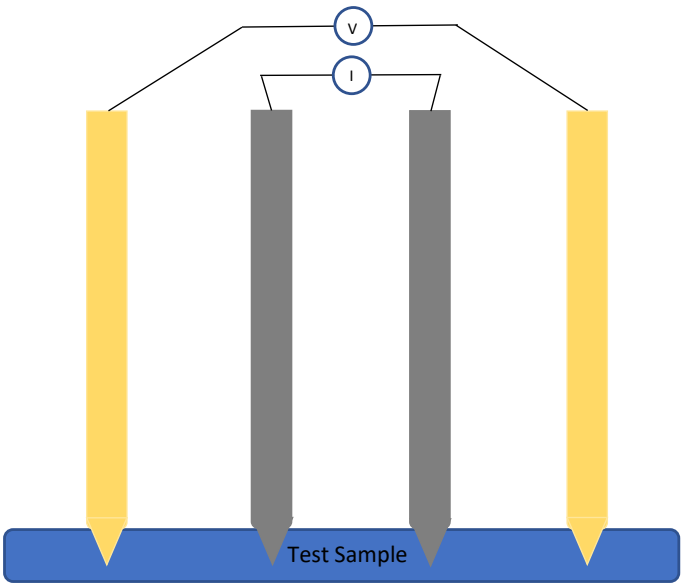

Figure 10: ***Schematic Representation of Four-probe Method:*** *The outer electrodes (yellow) are set as Voltage excitation electrodes while the resulting current is sensed by the inner electrode pair (grey)*

The difference between the Four-probe and Two-probe techniques is that the role of source and readout is assigned to two different electrode pairs in the former unlike how both roles are played by a single pair in the latter [35].

Conventionally, the outer two electrodes act as the source connections responsible for providing the test voltage, and the inner two electrodes serve as the readout pair, responsible for recording the current flowing through the device in response to the test voltage and giving the resistivity value (Figure 10). This method provides more accurate readings. By separating the source and readout connections, the chances of the addition of the internal resistance to the actual measurement are significantly less. This is because the current does not flow through the source pair.

4 BIOIMPEDANCE ANALYSIS

Monitoring the TEER of the cell cultures helps in the assessment of the tightness of the tissue barrier and the integrity of the tight junctions. To measure the TEER and changes in it, impedance analysis is often used.

As discussed in **chapter 3**, the cell can be represented as an analogous electrical circuit as shown in Figure 9. The electrical response study of the cells is known as bioimpedance analysis.

The organ-on-chip devices with integrated electrodes for TEER measurements are in essence two-port systems. Two terminals constitute one port. In the case of Organ-on-chips (OoCs), each electrode represents a terminal. The terminals satisfy the port condition: the electric current applied as an input in one terminal is equal to the current emerging from the other terminal on the same port [36].

A simple representation of the two-port network [36] is shown in Figure 11 with port definitions. The ports act as interfaces where the network connects to other networks. They are positions where signals are applied or the required output is measured. Conventionally, port 1 is considered the input port and port 2 is considered the output port.

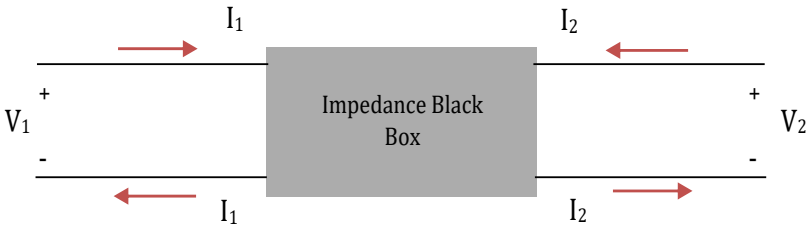

Figure 11: **A Schematic Representation of a Two-Port Network:** *The impedance black box represents the impedance circuit of the two-port network. V_1 and V_2 represent the voltage drop across the two port terminals. I_1 and I_2 are the currents applied to the two terminals and in a two-port network, the same current that is applied at the input of one port is obtained at its output. The value of the impedance of the black box, which is called the transfer impedance, can be calculated through a set of relations obtained by setting either of the two terminals as an open circuit. Figure based on the schematic representation by Gray et al. [36]*

The impedance black box shown in Figure 11 can be replaced by the appropriate circuit of interest. In this case, it is the impedance circuit which constitutes the different parts of the OoC (Figure 12). The electrical equivalent circuit comprises of the contact impedance of the electrode (Z_{el}), the impedance of the top (Z_{top}) and bottom (Z_{bot}) channel medium and the impedance of the cell layer (Z_{cell}).

The electrode impedance is due to the double-layer capacitance generated at the electrode-electrolyte interface and is hence capacitive. The media used for perfusion in the channels of the OoCs, although being highly conductive, has an electrically resistive nature.

The biological cell layer can be represented as a simple parallel RC circuit. The tight junctions of the cell barrier represent the resistive component and the cell

membrane represents the capacitive component of the cell layer impedance. The frequency-dependent behaviour of the circuit model is explained in section 3.2.

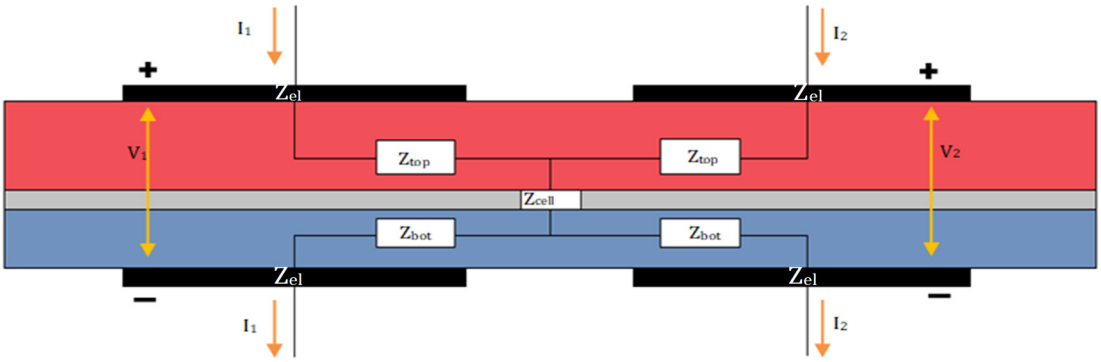

Figure 12: **A Simple Representation of an Organ-on-Chip as a Two-Port Network:** *An Organ-on-chip with integrated electrodes can be represented as a two-port network with the excitation and read-out electrodes acting as terminals. The black box shown in Figure 11 can be replaced by the impedances of the different layers of the chip which includes the double-layer impedance developed at the electrode-medium interface (Z_{el}), the impedances of the media at the top (Z_{top}) and bottom (Z_{bot}) channel layers and the cell layer impedance (Z_{cell}).*

In OoCs, the cell culture is done on porous membranes and the membrane pores act as resistive paths which add to the measured impedance other than the resistance of the perfused media.

In most OoCs, the four-point measurement or four-probe method is implemented. The excitation is provided via current-carrying (CC) electrode pair or pairs. The output voltage is detected by voltage-sensing pickup (PU) electrodes. The ratio of the voltage detected at PU and the current provided at CC provides the measured impedance.

When input current (I) is provided at the CC electrode, it results in a current density field (J). The density field results in a potential field to develop in the top channel of the OoC. The field lines cause the ionic transfer in the cell layer which results in the voltage drop across the layer [37]. The magnitude of current passing through the layer is equal to the input current but the amount of current passing through the resistive tight junction path and that through the capacitive cell membrane path depends on the frequency.

4.1) Current Sensitivity Distribution

If a current I is injected to the CC electrodes, it generates a current density vector J_1. If the same current I is injected to the PU electrodes, it generates another current density vector J_2 and following the reciprocity theorem these two densities are equal [38]. The two density fields are used to calculate the sensitivity distribution across the cell layer.

A change in resistivity of the cell layer will result in a measurement of the change in impedance by [39],

$$\Delta Z = \iiint S \times d\rho \times dv \ [\Omega] \tag{5}$$

Where ΔZ is the change in measured impedance magnitude in Ω, S is the sensitivity in m^{-4}, $d\rho$ is the change in resistivity of the cell layer in Ω·m and dv is the volume element in m^3. S provides the accuracy of the measured change while the change in resistivity provides the variation in the measured signal.

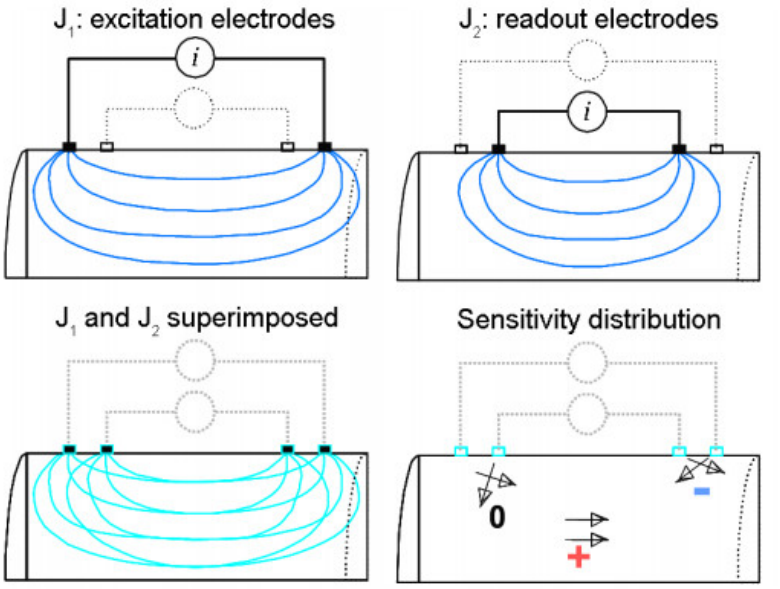

Figure 13: **Schematic representation of the distribution of current sensitivity in a four-terminal impedance measurement:** *The electrical field developed due to the applied current in the excitation electrodes is superimposed with the electric field that is generated when the same current is applied to the readout electrodes (as per the reciprocity theorem). If the fields align with each other, the resulting sensitivity is high, if the fields are perpendicular the resulting sensitivity becomes 0; and the resulting sensitivity is negative if the fields are oppositely directed. Adapted from Kauppinen et al. [40]*

The sensitivity(S) is calculated by the formula [41],

$$S = \frac{J_1 . J_2}{I^2} \ [m^{-4}] \tag{6}$$

Where all symbols represent the parameters discussed before.

To understand how each part of the cell layer contributes to the measured impedance, the sensitivity is normalized (S_n) by multiplying it with the square of the cross-sectional area (m^4) of the cell layer (A).

$$S_n = \frac{J_1 . J_2}{I^2} \times A^2 \ [1] \tag{7}$$

Ideally, S_n should be equal to 1 (a change in resistivity results in an equal change in measured impedance) throughout the cell layer which indicates the uniform contribution of each part of the cell layer to the measured impedance. Since,

$$J_1 = J_2 = \frac{I}{A}$$

$$\Rightarrow J_1.J_2 = |J_1|^2 = |J_2|^2 = \left(\frac{I}{A}\right)^2$$
$$\Rightarrow \frac{J_1.J_2}{I^2} \times A^2\,[1] = 1$$

(8)

In most cases, OoCs implement multiple small CC and PU electrodes. Each of these electrodes generates their current density field when an input current is injected into them. Each field has magnitude as well as direction. When they superimpose, it results in a field with regions where the fields get cancelled out, diminished or amplified [40].

The non-uniformity of the field lines results in non-uniform distribution of the current in cell layer volume. This leads to the measured impedance of the cell layer to be estimated higher in some parts of the cell layer (S_n>1) and lower in others (S_n<1). There may also be negative sensitivities present [37] which indicates a decrease in measured impedance to an increase in resistivity. This happens if the angle between the density vectors is >90°.

It is to be noted that using such a system, the measured impedance is the transfer impedance of the two-port network. It is the transfer factor between the input and output ports. As *Grimnes et al.* [37] states if impedance measured is equal to zero, this is not because the tissue volume is well conducting, but due to no signal transmittance from the CC to the PU electrodes.

4.2) The Dependence of Sensitivity Field on Electrode Dimensions

The positioning of the electrodes influences the measuring depth as stated by *Grimnes et al.* [37]. If the electrodes are driven from a constant voltage source, the current density will diminish with an increase in the distance between the CC and PU electrodes. However, the relative contribution of deeper layers of the concerned tissue volume will increase.

The sensitivity (S) is proportional to the current density squared (J^2), and thus the portion of tissue close to the electrodes is of more concern for the desired result than the tissue in the deeper layers. This measuring depth can be altered by varying the distance between the electrodes. Additionally, the depth can be varied by utilizing a third CC electrode between the two measuring electrodes [42].

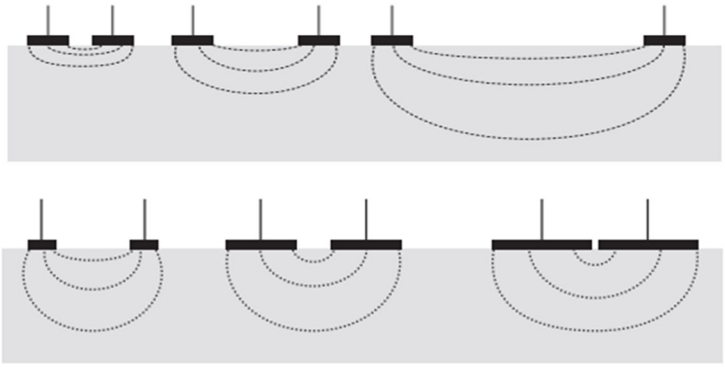

Figure 14: **Variation of measuring depth with electrode position and width:** *(top) The further the CC and PU electrodes are placed; more is the measuring depth. Thus, a correct separation must be used to achieve the desired depth, (bottom) the measuring depth is not heavily dependent on electrode width. However, a region of high sensitivity is developed in the region of the narrow gap between the CC and PU electrodes which can lead to higher estimation of results. This can be reduced by keeping the narrow gap fixed and decreasing the electrode width. Adapted from the book on Bioimpedance by Grimnes et al. [37]*

Electrode dimensions however do not heavily affect the measuring depth [37]. It is shown in Figure 14 for electrodes with different areas but equal electrode centre distances. A narrow gap between two adjacent electrodes will lead to a high sensitivity there. However, the number of tissue voxels is less and the number of low sensitive voxels in the overall volume is very high. The sensitivity can be improved by keeping a narrow gap, but decreasing the area of the electrode surface. Multiple surface electrodes can also reduce the measuring depth. The electrodes are commonly integrated in the form of metal strips and the measuring depth is determined by the strip width as well as the distance between the strips [37]. The study by *Yeste et al.* [27] as discussed in **chapter 2** becomes particularly important in this aspect.

Hence, it can be concluded that optimum electrode configuration is crucial to perform proper TEER measurements of cell culture.

5 ORGAN-ON-CHIP MODELLING

For the thesis assignment, the task is to design an electrode system for organ-on-chips so that it can be used for simultaneous measurement of Transendothelial Electrical Resistance (TEER) of cells cultured on porous membranes inside multiple channels in Organ-on-chips.

To take up the task at hand, the idea was to first do simulations on a 2D model of the channels of the chip to be designed. The electrodes were also designed in the model and COMSOL Multiphysics® v5.4 was used to do the simulation studies.

When it comes to electrodes, the main issue that arises is to decide on the width of the electrode surface and the separation of the excitation and readout electrodes. Another problem is to figure out what type of measurement to use, the main options, in this case, being, two-point measurement and four-point measurement.

One other important consideration is that the electrodes should be positioned to ensure as uniform a sensitivity distribution in the cell layer as possible. As discussed in the previous chapter under **section 4.2**, the electrode dimensions and positioning affect the generated sensitivity fields.

Although transparent and semi-transparent materials such as glass are available for electrode fabrication, the approach for the design and modeling used was for a more general case. Hence, the space between the electrodes was also kept such that it assures proper visibility of the cell layer under the microscope. So, the electrodes cannot be made too wide and, the separation of electrodes should be such that a balance is obtained between the output response and the visibility of the cell layer.

5.1) The Design of the Model

For the COMSOL Multiphysics® Simulation, a 2D design was used. The chip comprises of a top channel (height = 650μm) and a bottom channel (height = 200μm). In between the channels, cells are to be cultured on a porous membrane. For simplicity, the membrane is not taken into consideration for the simulations. The cell layer is given a height of about 10μm for the simulation. The length of the channels and the cell layer is set as 5mm and their width has been considered as 500μm.

A total of 6 pairs of electrodes are used. Four pairs have a width of 300μm and two pairs (at the middle) have a width of 100μm. The electrodes are positioned in such a way that the distance between the centre of two adjacent electrodes is 650μm (see Figure 15).

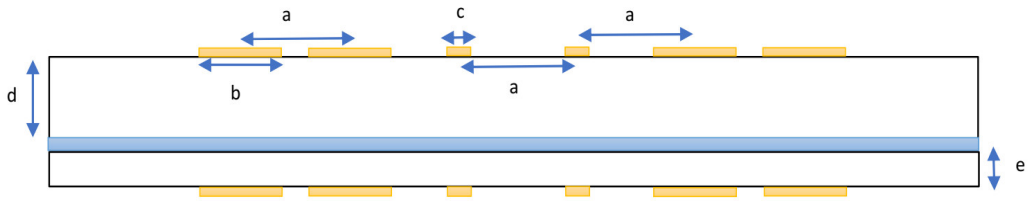

Figure 15: **The 2D design used for COMSOL Multiphysics® Simulations.** *The electrodes used are of two different widths b (= 300µm) and c (= 100µm). The electrodes are distanced from each other such that the centres of two adjacent electrodes are kept at a separation of a (= 650µm). The top channel has a height of d (=650µm) and the bottom channel has a height of e (=200µm).*

This is done based on the findings of *Yeste et al* [27] that the normalized current sensitivity is found to be close to the ideal 1 with the least variations if the distance between the centre of CC and PU electrodes is close or equal to the height of the top channel.

At a time three pairs are used as current-carrying electrodes of a four-point system and the other three as voltage sensing electrodes. In COMSOL Multiphysics®, two electric current (ec) studies are done where the electrode roles are interchanged.

5.1) The Considerations for the Simulation

To perform the study on the electrical response of the cell layer and the sensitivity of the electrode system, the AC/DC module of COMSOL Multiphysics® v5.4 was used. The study was conducted using Electric Current (ec) study of the module.

To produce a frequency-domain study, a parametric frequency sweep from 10Hz to 10MHz was done. Another parametric sweep was used to vary the TEER of the cell layer from 10Ω*cm^2 to 1000Ω*cm^2 to simulate the growth of the cell layer from an undeveloped to a fully developed culture.

For proper simulation studies, the appropriate material properties were assigned to the concerned domain as can be found in *Table 1*.

The excitation is provided to the positive electrodes of the excitation pair by using terminals with a current of 10µA while the negative ones are grounded. The readout pairs are set as terminals with zero current and voltage.

Table 1- The Applied Material Properties

Parameter	Value
Height of cell layer (h_{cell})	10µm
Height of top channel (h_{top})	650µm
Height of bottom channel (h_{bot})	200µm
Width of channels and cell layer (w)	500µm
Conductivity of culture medium [43] (σ_{med})	1.67S/m

Relative Permittivity of culture medium (ε_{med})	80
Approximate cell layer capacitance [44] (C_{cell})	$4\mu F/cm^2$
Approximate double-layer capacitance [45] (C_{dl})	$20\mu F/cm^2$
Input current (I)	$10\mu A$

To implement the variation of conductivity of the cell layer (σ_{cell}) with TEER, the conductivity was defined as a variable quantity [27]:

$$\sigma_{cell}[S.m^{-1}] = \frac{Height\ of\ cell\ layer\ [\mu m]}{TEER\ [\Omega * cm^2]} \tag{9}$$

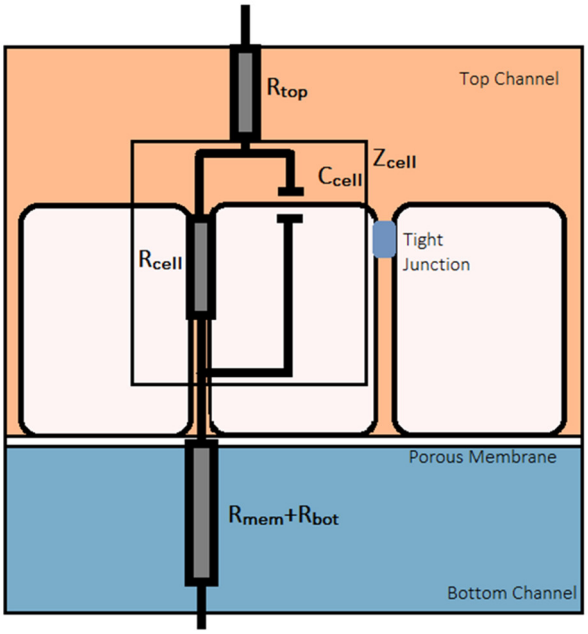

Figure 16: **The electrical equivalent circuit of a cell cultured on a porous membrane:** *The cell membrane represents an electrical capacitor (C_{cell}) while the tight junctions represent resistive paths of the cell (R_{cell}). The media flowing through the channels and the porous membrane also have a certain resistance which are represented as R_{top}, R_{bot} and R_{mem} for the top channel, bottom channel, and membrane respectively. In case of DC applications, only the resistive path of the tight junction is considered. If frequency domain AC studies are to be conducted, then the capacitive nature of the cell also needs to be taken into consideration.*

The biological cell can be represented as a simple parallel RC circuit (Figure 16) in the case of AC frequency-domain studies. The net impedance of the cell layer was assigned to the cell layer domain as,

$$|Z_{cell}|[\Omega] = \frac{1}{\sqrt{\left(\frac{1}{R_{cell}}\right)^2 + (\omega C_{cell} A)^2}} = \frac{1}{\sqrt{\left(\frac{A\sigma_{cell}}{h_{cell}}\right)^2 + (2\pi f C_{cell} A)^2}} \tag{10}$$

Where, Z_{cell} is the cell layer impedance in Ω , R_{cell} is the resistance of the cell layer in Ω which represents the tight junctions, C_{cell} is the cell layer capacitance in F/m^2 which represents the cell membrane, f is the frequency of the applied signal in S/m , σ_{cell} is the cell layer conductivity in S/m as defined in equation (9), h_{cell} is the height of the cell layer (m) and A is the cross-sectional area of the layer (m^2).

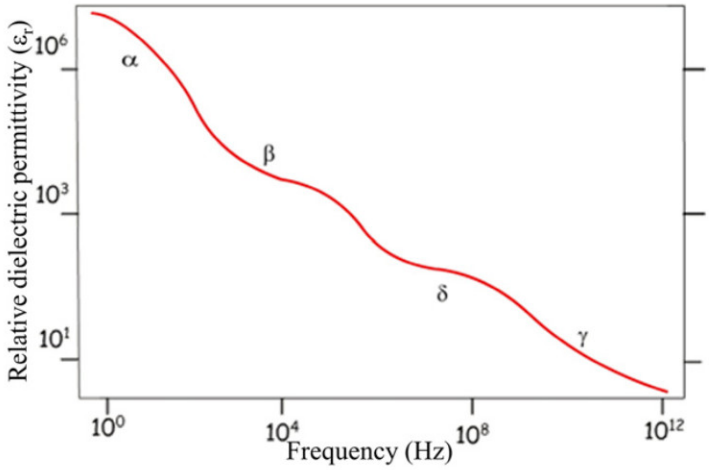

Figure 17: **The frequency dependence of relative permittivity of biological tissues:** *The plot shows the typical frequency dependence of the relative permittivity of biological tissue. The permittivity value gradually decreases with an increase in frequency. Adapted from Farsaci et al. [46]*

As the study is done in the frequency domain, it is required to consider the complex nature of the permittivity [46-47]. The relative permittivity of tissues decreases with an increase in frequency as shown in Figure 17. This consideration is made in the model using the relationship [48],

$$\varepsilon_r = \frac{\varepsilon'}{\varepsilon_0} - j\frac{\sigma_{cell}}{2\pi f \varepsilon_0} \tag{11}$$

Where, ε_r is the relative permittivity of the cell, ε' is the real permittivity of the cell and ε_0 is the permittivity of vacuum. The real part can be calculated from the cell layer capacitance.

In addition to the cell layer impedance, the model also needs to consider the resistive medium channels. The design comprises of a top and a bottom channel with heights h_{top} and h_{bot} respectively. The resistances of these layers are defined as,

$$R_{top}[\Omega] = \frac{h_{top}}{A\sigma_{med}} \tag{12}$$

$$R_{bot}[\Omega] = \frac{h_{bot}}{A\sigma_{med}} \tag{13}$$

Where R_{top} and R_{bot} are the resistances of the top and bottom medium channel layers in Ω.

The double-layer capacitance developed in the electrode-electrolyte interface results in the generation of impedance which is represented as,

$$Z_{el}[\Omega] = \frac{1}{j2\pi f C_{dl} A_{el}} \quad (14)$$

Where, Z_{el} is the electrode impedance generated due to the double-layer capacitance in Ω, C_{dl} is the double-layer capacitance in F/m^2 and A_{el} is the area of the electrode surface in m^2.

5.2) Sensitivity Distribution Calculations

In section 4.1, the theory behind current sensitivity and the calculation of normalized sensitivity to understand the sensitivity distribution has been discussed. In the simulations, equation (7) has been used to calculate the distribution. COMSOL Multiphysics® v5.4 derives the values of J_x and J_y which are the x and y components of the current density generated in the simulations. The calculations of equation (7) are done using these components.

Two separate Electric Currents (ec) studies are conducted. In one of the studies, certain pairs of electrodes are set up as the CC electrodes while the remaining pairs are set as PU electrodes. In the other study, the definitions of the electrodes are reversed. The electrodes can be defined as excitation and pickup in different ways and some have been explored to observe the changes in the results in the model.

5.3) Results and Discussion

The electrodes were defined in two different ways. The first way of defining was the conventional alternative CC and PU pairs along the length of the chip (Figure 18 top). The other way was to define the three pairs of electrodes on one side as CC pairs and the other three pairs on the other side as PU pairs (Figure 18 bottom).

In the case of the latter, the distance of the centres of the CC and PU electrodes are no longer equal to the height of the top channel instead of the last CC pair and the first PU pair (both with 100μm width). This was done to compare results and observe how different the obtained results can be if CC and PU electrodes were defined differently.

For both simulations, an extremely fine physics-controlled mesh was used which generated 8862 mesh vertices and 17426 triangular elements. A total simulation time of 4 minutes and 45 seconds was required for performing the frequency sweep study from 10Hz to 10MHz with a step size $10^{0.1}$Hz. The simulation time will increase or decrease with a corresponding increase or decrease in the step size.

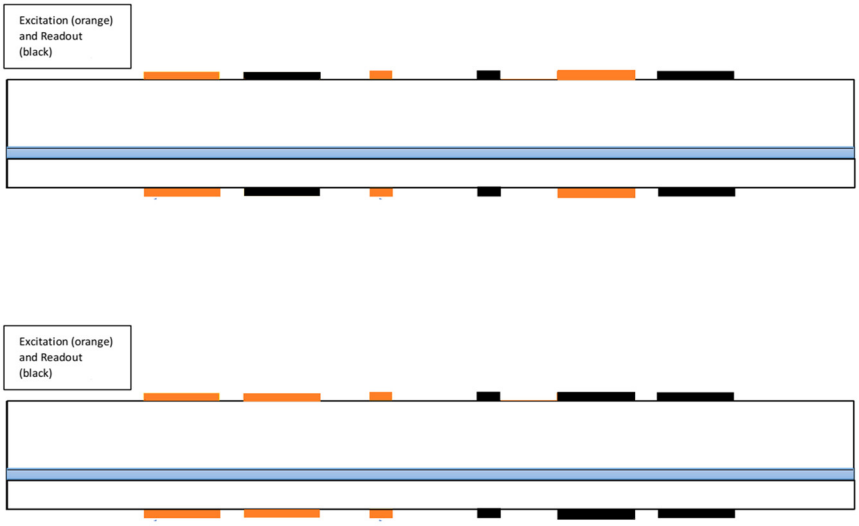

Figure 18: **The two different configurations used to define the electrode excitations:** *Configuration 1 (top): The alternate pairs of electrodes are defined as CC and PU electrodes. In this configuration, the separation of the centres of CC and PU electrodes is equal to the height of the top channel layer, taking into consideration made by Yeste et al. [27]. Configuration 2 (bottom): Three pairs of electrodes on one side of the chip are defined as CC electrodes and the other three pairs are defined as PU electrodes. In both pictures, orange represents the CC electrodes and black represents the PU electrodes.*

Figure 19 shows the normalized sensitivity distribution in the cell layer in the case of both configurations. In both cases, the plots were obtained by calculating along the length of a cutline passing through the centre of the cell layer domain. It can be observed that in the case of both configurations, the sensitivity distribution approaches uniformity as TEER increases.

In the case of the first configuration, there is a wide region where normalized sensitivity is greater than 1, which spans approximately 3mm of the channel with approximately 1mm long regions on either end of the channel which shows a drop of the normalized sensitivity to less than 1. The regions where the sensitivity is greater or less than 1 remain increases slightly with an increase in TEER values and corresponds with the region where the electrodes are located. However, the peak of the curve decreases with an increase in TEER. In case of the second configuration, the region where sensitivity is greater than 1 gradually increases with the curve peak decreasing with an increase in TEER. The region where the sensitivity is less than 1 correspondingly becomes smaller.

The sensitivity value indicates the change in the measured impedance due to the corresponding change in the conductivity of the material. This is indicated by equation (5). When the sensitivity is normalized, the deviation from $S_n=1$ determines the error in measurement due to overestimation or underestimation of the measurand.

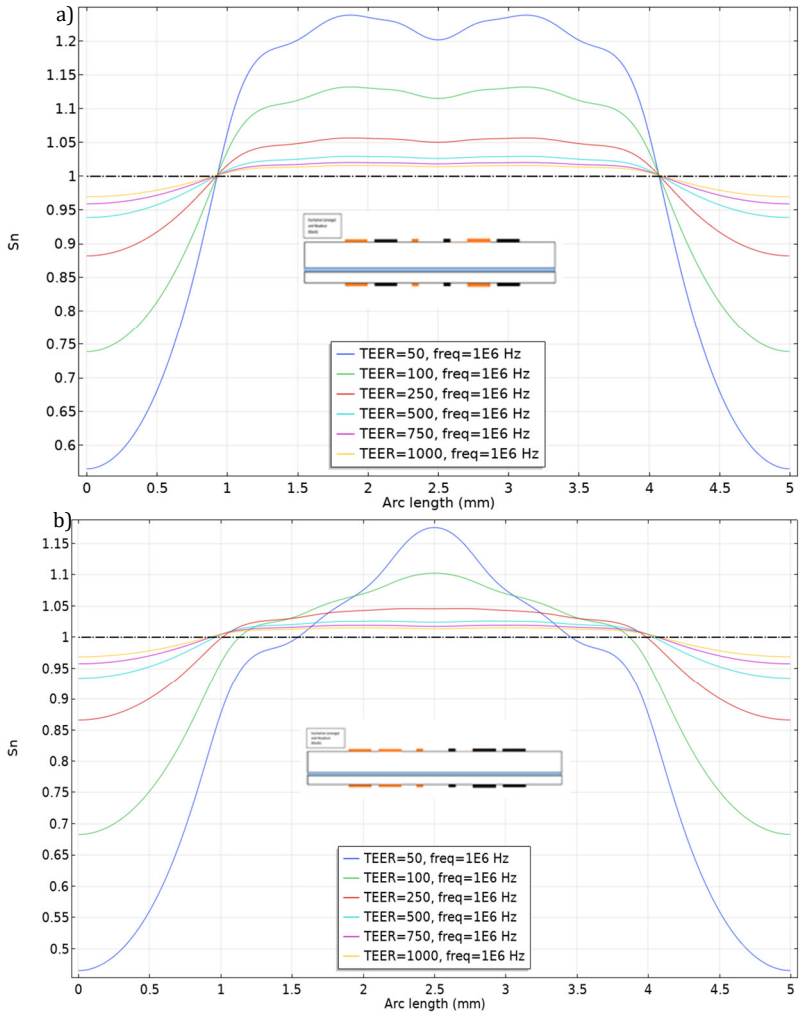

Figure 19: **Normalised Sensitivity Distribution obtained from COMSOL Multiphysics® simulations:** *The normalised sensitivity distribution obtained for Configuration 1 (a) and Configuration 2 (b). In both cases, no portion of the cell layer contributes to uniform sensitivity of 1 which is represented by the dotted line. The sensitivity is higher than 1 in the regions where the electrodes are located and gradually decreases and falls below 1 towards the channel ends.*

In Figure 19a, when alternating pairs are defined as CC and PU electrodes, the normalized sensitivity reaches a highest of 1.243 (measured signal is +24.3% than actual value) at two positions for 50Ω*cm^2 corresponding with the regions of the wider electrodes. The sensitivity shows a dip in the narrow gap between the two smaller electrodes. Beyond the regions of the electrodes, the sensitivity gradually drops to a minimum of 0.567 at the two ends of the channel where the measured signal is -43.3 % than the actual value of the impedance. A similar trend is seen for higher TEER with the peak sensitivity gradually decreasing and approaching uniform sensitivity distribution. The peak sensitivity decreases to 1.0165 for 1000Ω*cm^2 and the sensitivity at the ends of the channel increases to 0.9703. This indicates an overall less erroneous measurement of the higher TEER values along the length of the cell layer while measured impedance will probably have higher errors for lower TEER values or less developed cell cultures. All results shown are at a frequency of 1MHz.

When this is compared to the second electrode configuration, the sensitivity distribution (as shown in Figure 19b) in case of lower TEER values shows a different trend. At 50Ω*cm^2, the region where S_n>1 is about 2mm which is less than the previous configuration. The curve shows a single peak in the region of the narrow gap between the excitation side and the readout side of the channel. The peak sensitivity indicates a measurement which is +17.576% than the actual value of the impedance in that region. This overestimation is significantly less than the overestimation shown in case of Figure 19a. The measured value drops to about -2% in the region just beyond the right and left most electrode pair and then gradually drops to -55% at the ends of the channel. This indicates a much higher underestimation at the channel ends than the first case.

As the TEER value increases, like the former configuration, the peak sensitivity gradually decreases and the amount of underestimation at the channel end decreases. This leads to a much less erroneous measurement in higher TEER values. Additionally, the nature of the curve gradually changes with increasing TEER, and the nature of distribution in both cases become almost identical for 1000Ω*cm^2.

In all cases of TEER, no portion of the cell layer was found to contribute to the ideal case of uniform distribution (S_n=1).

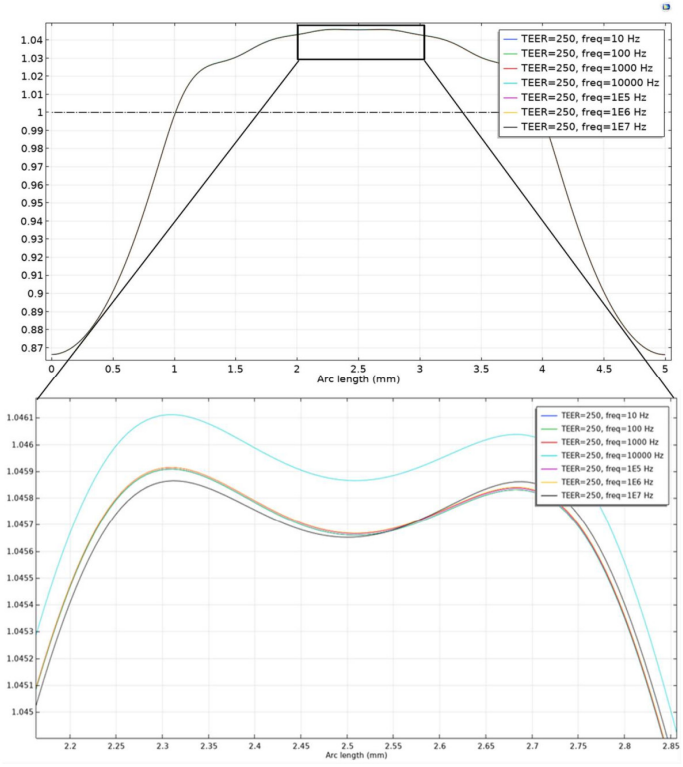

Figure 20: **The variation of Normalized Current Sensitivity with frequency:** *All results shown for TEER of 250Ω*cm^2. The dotted line indicates the ideal normalized sensitivity of 1. The variation obtained is very small as can be seen from a zoomed-in view of the plot peaks.*

To observe the effect of the variation of frequency on the current sensitivity, the normalized sensitivity was plotted for 250Ω*cm^2 (see Figure 20). The variation of response with frequency was found to be very low with the peak overestimation varying between +4.6% (for 10000Hz) and +4.505% (for 10MHz). The variation becomes less with an increase in TEER values.

The non-uniform distribution of sensitivity is due to the electric potential field generated in the upper channel layer of the chip. The distribution would be uniform if there were equipotential lines in the field all along the length of the cell layer. This would lead to an equal distribution of the current per unit area of the cell layer. However, this is an ideal case, and owing to the use of multiple electrodes, superposition of all the individual density fields, the electrical properties of the channel medium, etc, the potential field may not contain equipotential lines everywhere.

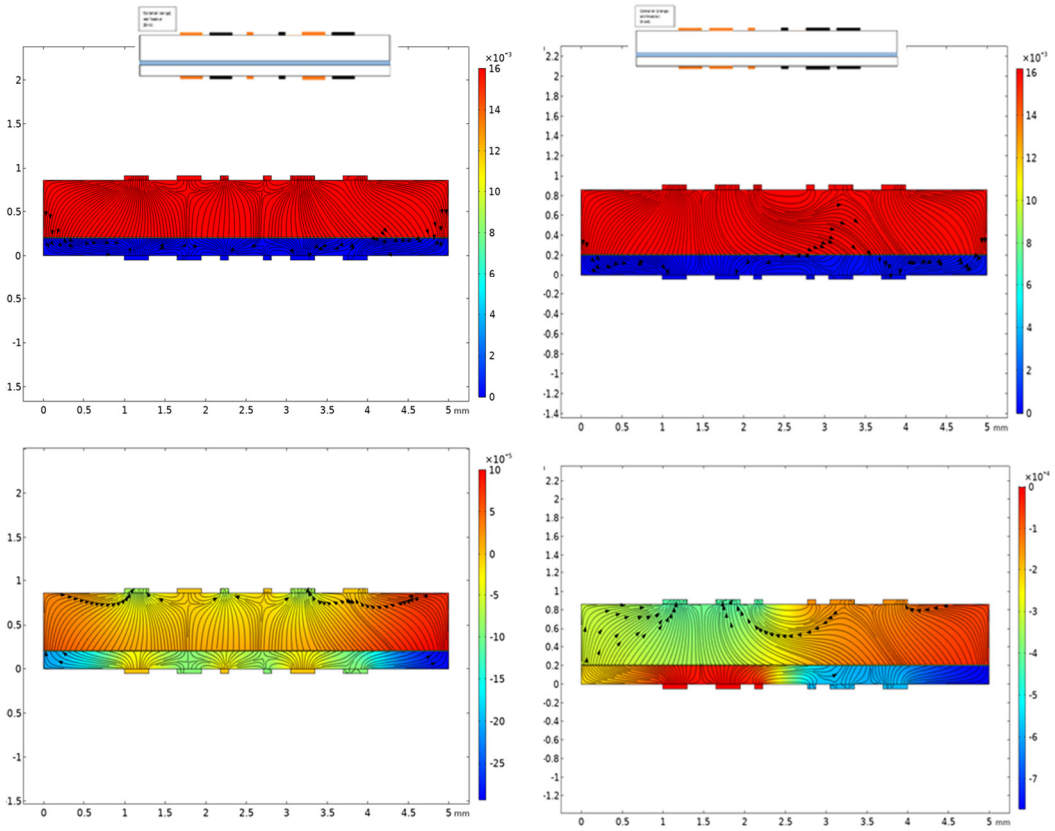

Figure 21: **The Generated Potential Field and Current Streamlines:** *The potential field generated inside the chip due to the input current is shown along with the current streamline for both configurations 1 (left panel) and 2 (right panel). No equipotential field lines are obtained above or below the cell layer leading to non-uniform sensitivity distribution. All results are shown for 1000Ω*cm^2 and frequencies (top to bottom) 1000Hz and 10000Hz.*

Figure 21 shows the potential fields and the current streamlines for both the configurations with the left panel showing that for 1000Ω*cm^2 at 1000Hz and 10000Hz for the first configuration. The right panel shows the same for the second configuration. It was found that the field does not remain uniform throughout the length of the cell layer resulting in the variation in distribution and non-uniform

impedance measurement. It is also found that at high frequency, there is a change in the electrode polarity.

When the normalized sensitivity is multiplied with the resistivity of the cell layer, the measured resistance along the cell layer is obtained. At 50Ω*cm^2 and 10000Hz, the measured resistance of the cell layer was obtained as 2486.5Ω at the two peaks and as 1135Ω at the two ends in case of the first configuration. The actual resistance is 2000Ω. For the same conditions, the highest resistance measured in case of the second configuration is 2351.3Ω which is a smaller overestimation than the former. The lowest measured value however is 931Ω which is a higher underestimation at the channel ends (See Figure A.1 in Appendix).

To better understand the performance of the two configurations in terms of measurement, the mean resistance was measured at each TEER value, and the standard deviations were calculated. This is shown in Table 2.

Table 2-Analysis of Results of the Two Configurations at 1MHz

Configuration	TEER (Ω*cm^2)	Mean Measured Resistance (Ω)	Actual Resistance (Ω)	Standard Deviation from Mean (Ω)	Error in Measurement (%)
1 	50	2020.8	2000	507.96	1.04
	100	4010	4000	588.60	0.25
	250	10003	10000	649.88	0.034
	500	20012	20000	673.25	0.059
	1000	40060	40000	685.95	0.15
2 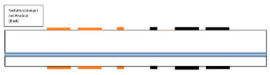	50	1725.2	2000	481.06	-13.74
	100	3756.1	4000	593.04	-6.1
	250	9847.8	10000	665.32	-1.52
	500	19928	20000	685.42	-0.36
	1000	40040	40000	693.78	0.1

The results shown in Table 2 provide a better comparison of the results. In case of configuration 1, the mean measured resistance is higher than the actual cell layer resistance in all cases. In comparison, configuration 2 shows an underestimation of the cell layer resistance in the measured mean except in case of 1000Ω*cm^2. Configuration 1 has a higher standard deviation for 50Ω*cm^2 but shows less deviation from the mean in cases of other TEER values compared to configuration 2. These indicate overall less variation from the mean measurements in the former.

Although configuration 1 overestimates the cell layer resistance, the percentage error indicates a much less erroneous result overall than configuration 2. The latter shows a slightly less error in case of 1000Ω*cm^2.

As per equation (4), the cell layer impedance spectra can be obtained by multiplying the magnitude of the impedance obtained with the phase component of the impedance. The resulting spectra for configuration 1 are shown in Figure A.2a and configuration 2 are shown in Figure A.2b in Appendix.

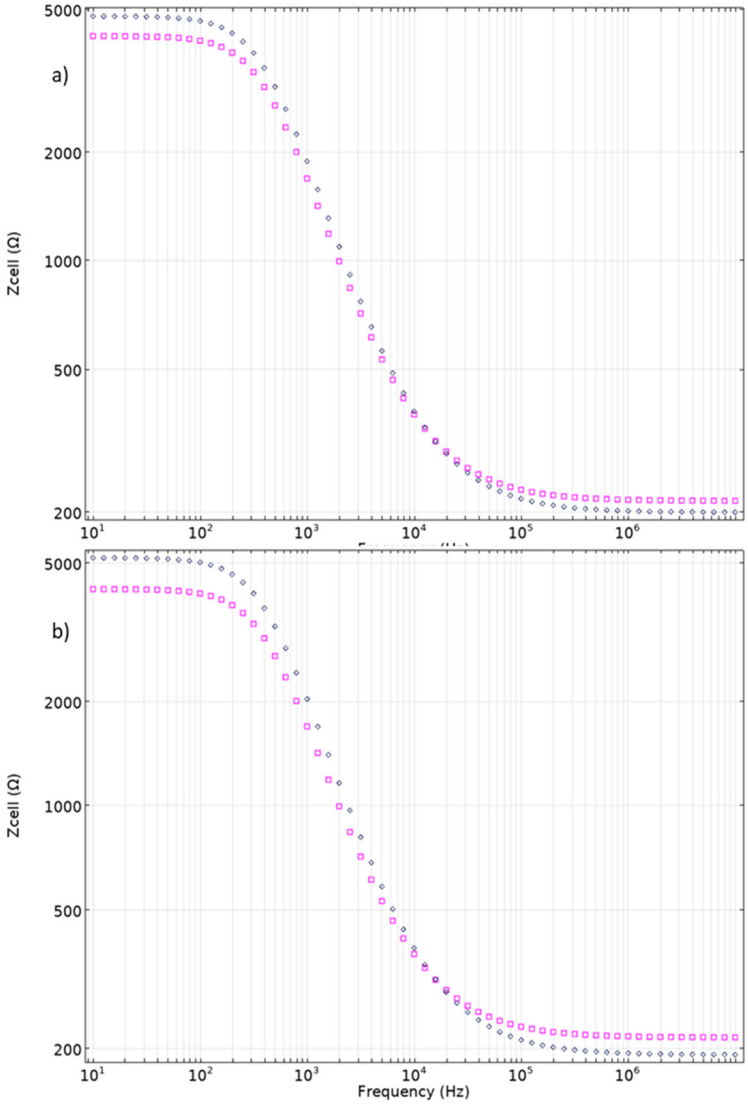

Figure 22: **Comparison of the Simulated Impedance Spectrum (black) and Actual Impedance Spectrum (pink) of the cell layer for 100Ω*cm^2:** *a) The spectra for Configuration 1, b) The spectra for Configuration 2.*

Figures 22a and 22b compare configurations 1 and 2 respectively where the simulated impedance spectrum is shown in black for 100Ω*cm^2 with the actual impedance spectrum is shown in pink. From the figure, it can be observed that for both configurations, the measured impedance at lower frequencies is overestimated. The measurement differences in the lower frequencies are higher for configuration 2 than that in case of configuration 1, e.g., at 10Hz, the differences

are 569.25Ω and 970.25Ω for configurations 1 and 2 respectively. At higher frequencies, beyond 10^4Hz, the measured impedance is found to be less than the actual spectral value, e.g., at 10^5Hz, the differences obtained are -13Ω and -20Ω for configurations 1 and 2 respectively.

5.4) Conclusions

It was found that the way the electrodes were defined influenced the nature of the sensitivity distribution along the cell layer. The mean cell layer impedance measured by the first configuration indicates an overestimation of the measurements for all TEER values while the second one shows an underestimation for all TEER values except 1000Ω*cm^2. However, the first configuration was found to be less erroneous compared to the other one which indicates that the former is the better choice of excitation. It also confirms the importance of fulfilling the requirement of having the distances of the centres of the CC and PU electrodes at a distance close to the top channel layer as suggested by *Yeste et al* [27]. Simulation results also show very low variations in the distributions with frequency which decreases as TEER increases. The distribution was seen to approach uniform distribution with an increase in TEER. The resultant impedance spectra also confirm that the electrode system will be able to measure the cell layer impedance more accurately if the first configuration is used. Although there are overestimations in the lower frequencies, the configuration measures the impedance for higher frequencies better with small errors.

5.4) Future Considerations

The sensitivity distribution can be improved by further altering the electrode geometry. Fabrication of electrodes with transparent material may enable the use of wider electrodes since then the electrodes will no longer block the visibility of the cell layers. Wider electrodes will lead to a smaller region where stray fields will influence the measurements. The performance of the system can also be improved by keeping the electrodes at closer proximity to the cell layer, i.e., by making the channel layers thinner. This, however, needs to be done keeping the ease of handling and aligning the layers of the chip in mind. The variation of electrode geometry can lead to changes in the sensitivity distribution which can be further refined by keeping the CC and PU electrodes as close as possible and by providing a proper balance in the electrode width and the narrow gap present in between the electrodes. This gap results in regions of higher sensitivity which can be reduced by using an additional CC pair between two measuring electrodes. The use of vertical electrodes to perform the measurements may also be an interesting approach. It is also to be noted that in this model, the cell layer is considered as a single continuous domain in COMSOL Multiphysics® for simplicity. This is not the case practically. A more accurate model of the cell layer can also improve sensitivity distribution.

6 THE DESIGN OF THE ORGAN-ON-CHIP

The results obtained from the COMSOL Multiphysics® model in **chapter 5** was used to design the OoC in SOLIDWORKS® 2019. This chip can be used for multiplexing and hence, would allow to perform different experiments simultaneously and measure the TEER of the cell cultures.

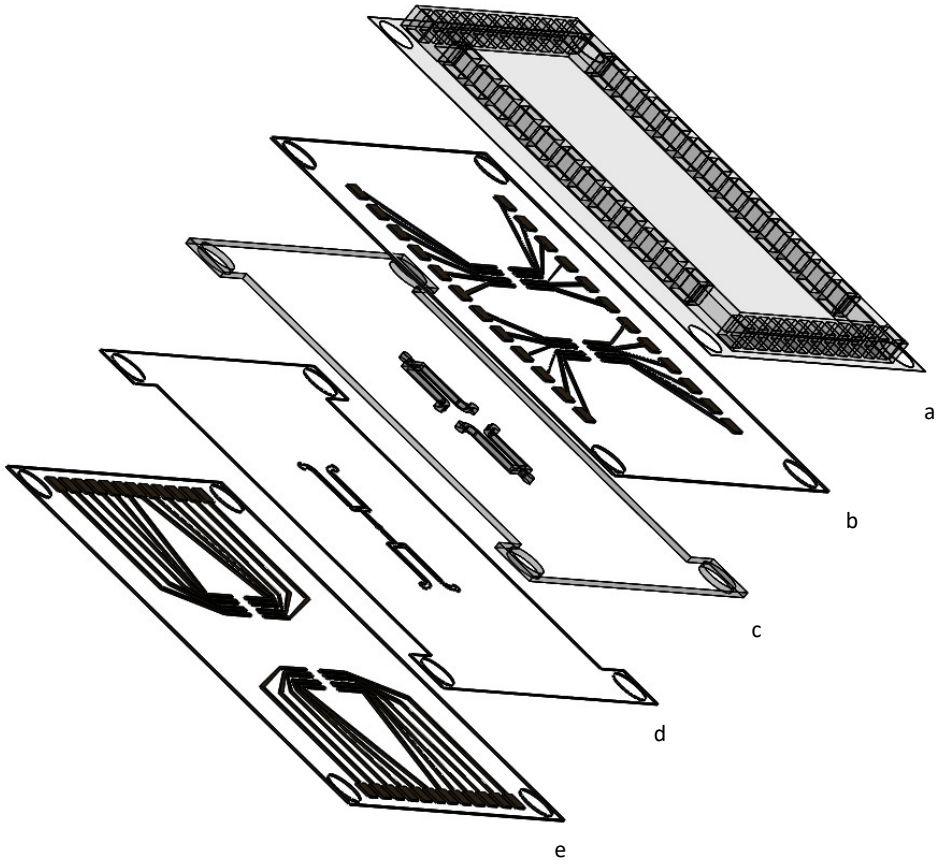

Figure 23: **The Exploded View of the Different Parts of the Organ-on-chip design:** *a) The topmost layer of the chip comprises of wire holders for assisting in connecting wires or jumper cables with the contact pads of the electrodes, b) the top electrode layer fabricated on a glass surface. The electrodes comprise of contact pads to establish connections with source, c) the top channel layer representing the perivascular compartment with four multiplexed experimentation channels, d) the bottom channel layer representing the vascular compartment with four multiplexed experimentation channels with common inlet, e) the bottom electrode layer fabricated on glass surface along with contact pads.*

The proposed chip design comprises of six different parts (Figure 23):

- Topmost layer with wire holders for making connections with electrodes.
- The upper electrode layer (250µm thickness).
- The upper channel for media perfusion (650µm thickness).
- Porous membranes for cell culture (~2µm thickness and not shown in Figure 23).
- The lower channel for media perfusion (200µm thickness).
- The lower electrode layer (250µm thickness).

The chip is 4.5mm in height, 50mm in length, and 48mm in width. It comprises of 4 multiplexed channels on the top and bottom channel layers. Flow is only desired for the bottom channel which represents the vascular compartment and to allow for simultaneous flow input in all the four channels of the layer, a common inlet is designed (Figure 24b). The medium applied in the inlet should distribute into the four separate channels simultaneously. Each channel is provided with its outlet which would allow for the individual access to the medium of each channel. This can be used to manipulate individual channel environments to perform different experiments.

The channel structure of the top channel layer is designed a bit differently than the bottom layer. Instead of a common inlet to all four channels, two inlets are designed with each being a common inlet to two channels (Figure 24a). This is done to separate the common inlet position of the bottom channel layer from that of the top channel layer and to provide easier access to each inlet. Since the membrane layer is porous, the alignment of the two channel layers is required to be such that only the experimentation channels of the structure are aligned to prevent intermixing of media right after their introduction through the inlets. The top channels also have their outlets like the bottom channels. The individual channel layers and the layers after alignment are shown in Figure 24.

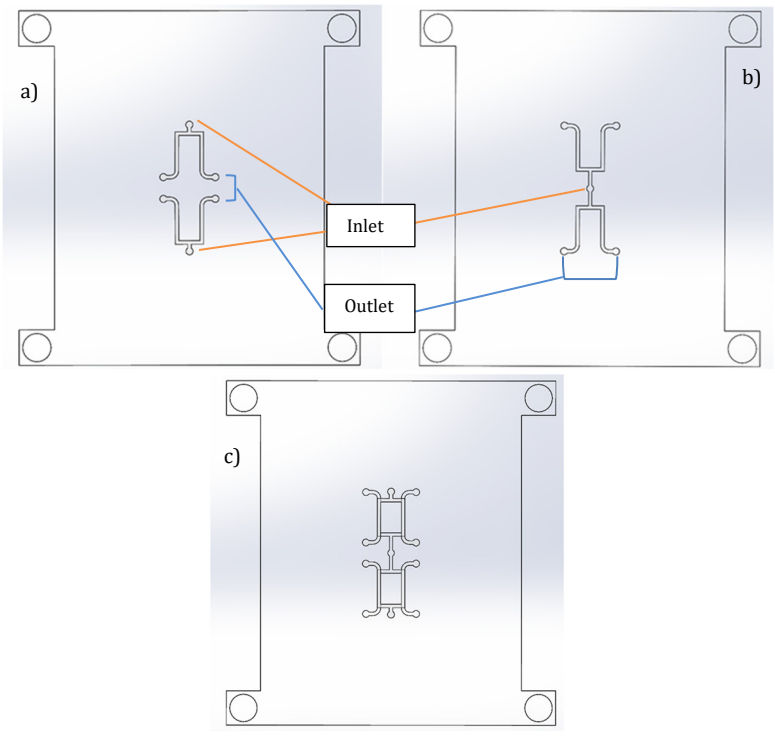

Figure 24: **The Two Channel layers:** *a) The top channel layer, b) bottom channel layer, c) the channel layers after alignment with each other and enclosing a porous membrane in between.*

Each channel is 5mm in length and 500µm in width. The top channel layer has a height of 650µm and the bottom channel layer has a height of 200µm. Each inlet and outlet has a diameter of 1mm. The inlets and outlets can be formed by punching holes in the marked positions after aligning the channel layers.

The electrode design and the positioning of each electrode along the individual channel lengths are done according to the COMSOL Multiphysics® simulation model used in **chapter 5**. The middle two electrode pairs have a width of 100µm while the other electrodes are 300µm wide. Each electrode is connected to a contact pad which can be used to provide positions for making wire connections.

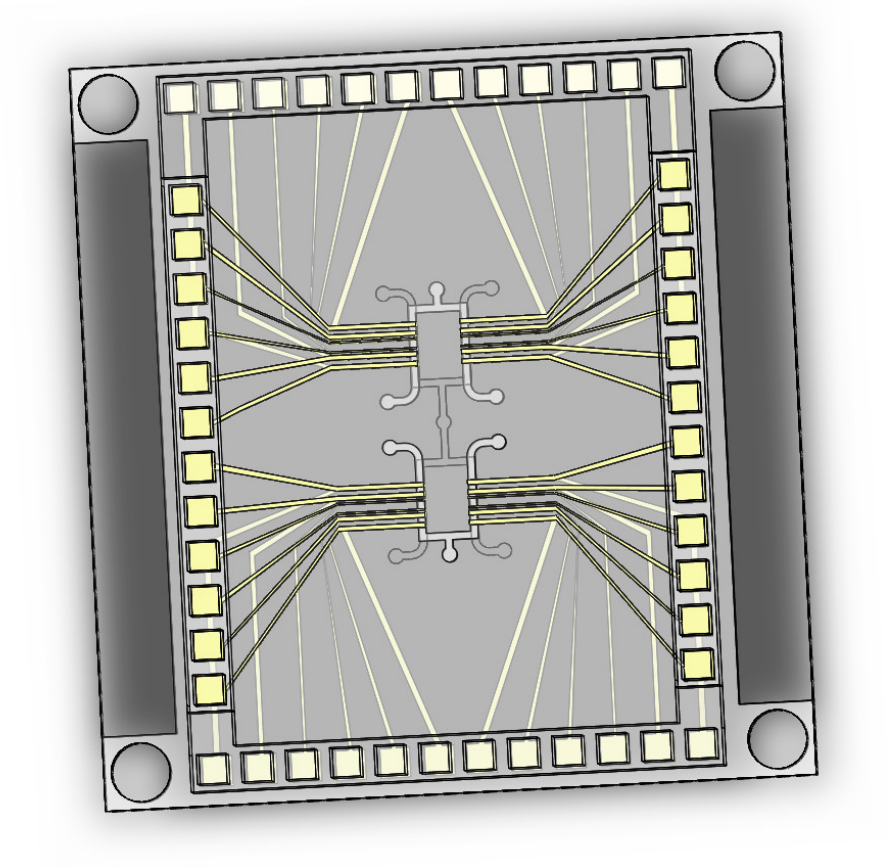

Figure 25: **The Assembled Design of the Organ-on-Chip**

Each aligned top and bottom channels along with the electrodes act as individual OoCs and hence, the chip comprises of 4 multiplexed OoCs. The assembled chip can be seen in Figure 25. The topmost layer comprises of wire holders with holes for access to the electrode contact pads (2mm x 2mm). Electrical connections can be made by fixing wires to the electrodes via contact pads using proper adhesive or fix jumper cables for making connections.

6.1) Fabrication of Channel Layers

Szydzik et al [49] proposed a one-step Injection moulding technique. This method requires the development of the complementary channel moulds of each layer. The two moulds are to be aligned as per desired with the porous membrane layer separating the two moulds.

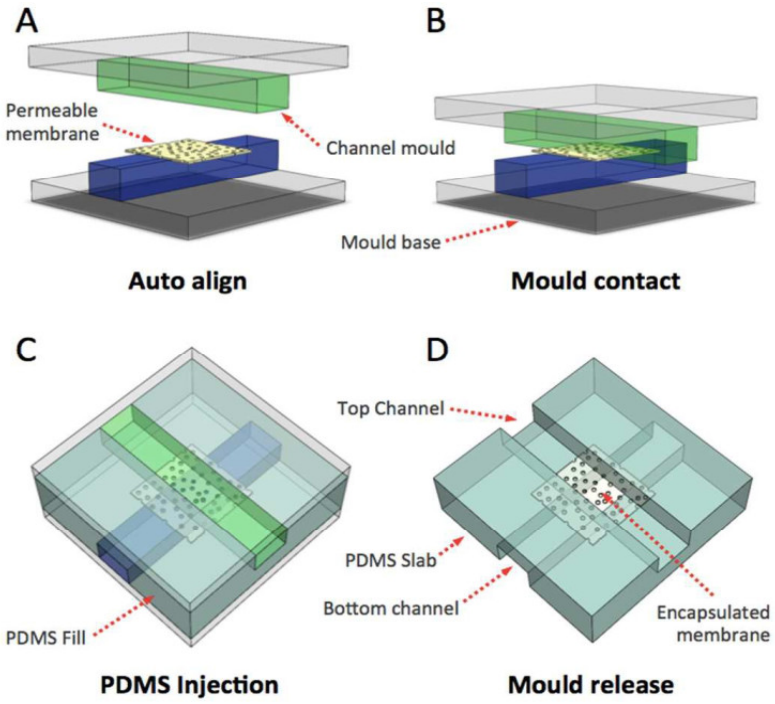

Figure 26: **One-step Injection Moulding Procedure for Fabrication of Microfluidic Structures:** *A) porous membrane is placed at the point of intersection of the channel mould structures, B) The mould structures are then brought into contact and clamped around the edges to hold them into place, C) PDMS is injected through an opening and the void between the structures is filled, D) PDMS infiltrates membrane portions which are not mechanically compressed, resulting in clear areas at the intersection of the channels. Adapted from Szydzik et al [49].*

PDMS will be injected in the space between the moulds to fill it up. Once the void between the moulds is filled up with PDMS, the two independent open channel layers will be formed with the membrane in between. Figure 26 A-D provides visualisation of this process (adapted from *Szydzik et al* [49]). To keep the moulds aligned and held in place, pressure can be applied to the edges of the moulds. Other than that holes can be punched on each corner of the mould's base and pins can be used to align them properly.

The moulds can be generated using standard photolithography microfabrication method [49]. A photomask with the design of the channel can be developed. This photomask can be used to generate the mould structure on a photoresist film placed on a silicon substrate. In this case, SU-8 is more widely used. SU-8 is a negative photoresist [50]. The portions of the material, when exposed to UV light, becomes cross-linked while the rest of the film can be washed away leaving behind the complimentary mould of the channels. Additionally, the moulds can be directly fabricated by using 3D-printing techniques [51]. This method can be used for rapid prototyping when the structures required to be produced are not of very high resolution. The minimum dimensions that can be printed, however, is defined by the resolution of the printer system used [49].

6.2) Flow Simulation-Results and Discussion

The SOLIDWORKS® 2019 model of the chip's bottom channel layer was imported to COMSOL Multiphysics® v5.4 to perform flow simulation studies. Flow is not required in case of the top channel which acts as the perivascular compartment and so flow characteristics is only checked for the bottom channel layer. The results of the simulation will provide an idea about the level of performance of the device. In case of a microfluidic platform based device, it is important to achieve an even flow and pressure distribution in the main channel branches to have identical experimental conditions in all the channels.

The simulation study is done keeping the Blood-Brain-Barrier-on-chip in mind and so the generation of the amount of shear stress is also looked into since the endothelial cells of the culture requires shear stress to be able to mimic physiological functions *in-vitro*. *In-vivo*, shear stress is expected to be about 0.5Pa [52].

For the study, the Laminar Flow (spf) physics was chosen. The common inlet and the outlets were input as the inlet and outlets of the physics respectively. The medium used is user-defined with a density of 1g/ml and dynamic viscosity(μ)of 1cPoise which is similar to that of PBS.

For the simulations, the following considerations are made:

- Incompressible flow
- No-slip wall condition
- Stokes' flow
- Shallow channel approximation with a thickness of 200μm.

For the generation of the mesh, a fine physics-controlled mesh was used which generated 135995 mesh vertices and consisted of 58712 triangular elements. A better quality mesh could not be used due to device constraints. A simulation time of 11 minutes and 15 seconds was required.

As stated before, shear stress of 0.5Pa is required to be present in each of the experimentation channels to be able to better replicate the *in-vivo* conditions *in-vitro*. That is why the flow rate required to achieve this is back-calculated using the equation [53],

$$\tau = \frac{6\mu Q}{wh^2}\ [Pa] \qquad (15)$$

Where τ is the shear stress in Pa, μ is the dynamic viscosity of the medium in Poise, Q is the volumetric flow rate in m^3/s , w is the width and h is the height of the channel in metres. By calculating, it was found that a flow rate of 4.76μL/s is required to be applied at the common inlet of the channels to have shear stress of 0.5Pa. This flow rate is applied as the input flow rate for the inlet in the model.

In Figure 27, a surface plot is shown to visualise the flow of the medium through the channel structure. The colour map plot shows almost an equal and symmetric distribution of flow in the channels. Ideally, each channel (marked in Figure 27 as 1-4) should have a flow rate equal to 50% of the rate at the inlet.

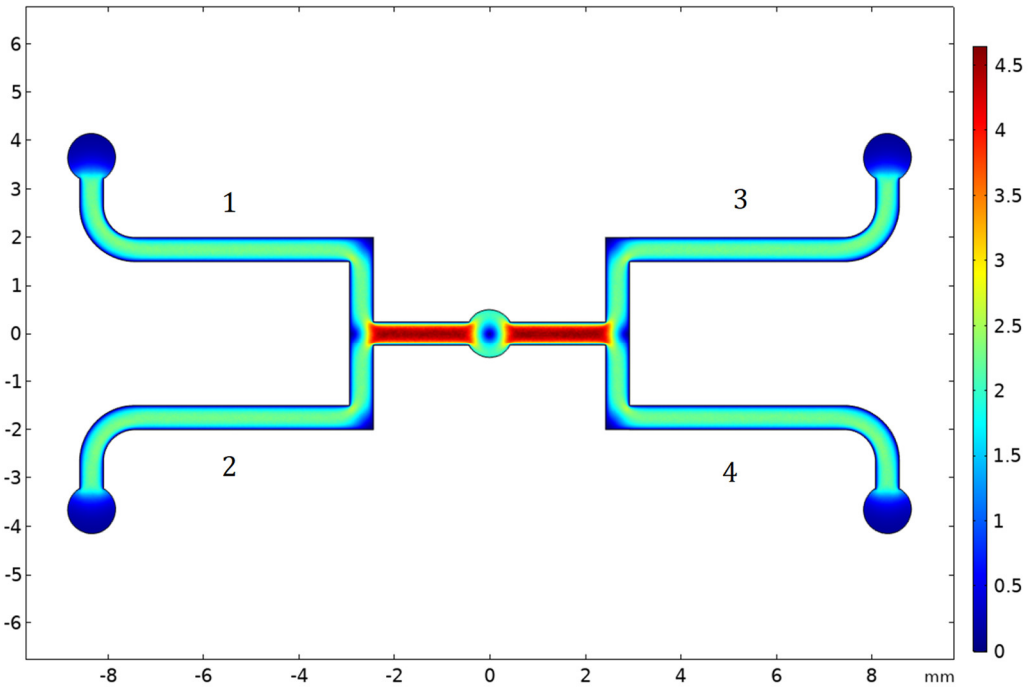

Flow Distribution			
Channel 1	**Channel 2**	**Channel 3**	**Channel 4**
49.8%	49.6%	49.51%	49.58%

Figure 27: **The Flow Distribution in the Channels:** *The figure shows a surface plot with colour map to show how the flow is distributed within the different branches of the structure. The table shows the percentage of the input flow rate obtained at each channel on distribution. The channels should ideally achieve 50% of the input flow rate which is not seen in any of the channels.*

To take a closer look into the distribution of flow, the flow rate was calculated along cut-lines passing through the centre of each channel, along its width. The table in Figure 27 indicates the percentage of the flow at the inlet that is distributed in that particular channel branch. It can be seen that there is a slightly non-uniform distribution of flow with all channels having a flow rate less than the expected 50% of the flow rate at the inlet. This is due to the hydraulic resistance of the channels which results in the drop of flow rate as the medium approaches the branches. One way to reduce this drop is to reduce the length of the portion of the channel that directs the medium from the common inlet to the branches.

Another way is to increase the cross-sectional area (height*width) of the channels. But there is a sort of limitation when it comes to varying the cross-sectional area. The aim is to have as uniform a shear stress as possible inside a rectangular channel. However, owing to the sidewalls of the channels, it is not possible to have it uniform all across as it will gradually drop to zero towards the walls. Thus, to

achieve a mostly uniform shear stress distribution along the width of the channel, the channel design must be such that the width of the channel is much greater than the height of the channel [22]. This will result in a flat flow profile for the case of this design where channel width (500µm) is much greater than the channel height (200µm). It can be seen that the flow has a parabolic flow profile which is expected and desired in microfluidics (Figure 28).

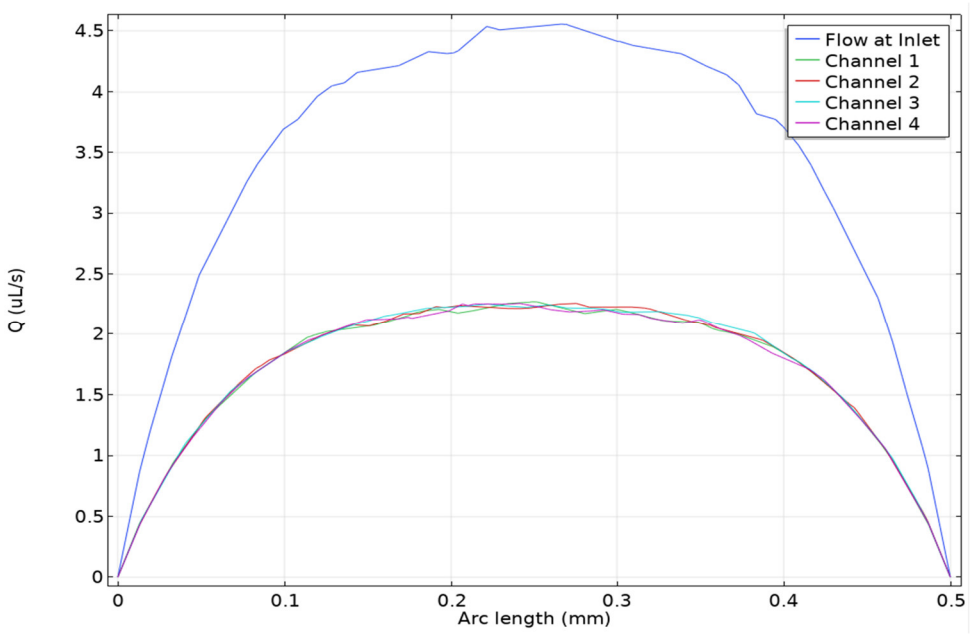

Figure 28: **The Flow rate at the Inlet and in each Channel after distribution:** *A flat parabolic flow profile is obtained within the channels with a maximum flow velocity near the centre of the channel and zero flow velocity at the side walls. The flow rate in each channel after the distribution is not the same but is more or less uniformly divided. The applied flow rate at the inlet was 4.76µL/s but simulation results show the flow rate drops instantly to 4.555µL/s.*

The percentage of flow rates achieved in each channel although indicates an overall drop in the flow rate, it shows that there is a more-or-less uniform distribution of flow in two adjacent channels (1-2 and 3-4).

Figure 29 shows the shear stress along the width of each experimentation channel plotted together. It is parabolically distributed along the width of the rectangular channels and is maximum near the channel middle while they decrease towards the sidewalls and becomes zero. The plot indicates that the shear stress is less than the expected value of 0.5Pa. This is due to the drop in the flow rate due to the channel resistance. The shear stress is also not equal in all channels. The value of the maximum shear stress is highest in channel 1 with a value of 0.477Pa and is lowest in channel 3 with a value of 0.4735Pa. This corresponds well with the amount of volumetric flow rate achieved in each channel, with channel 1 achieving the highest and channel 3 the lowest. The table in Figure 29 shows the value of simulated maximum shear stress in each channel until four places of decimal.

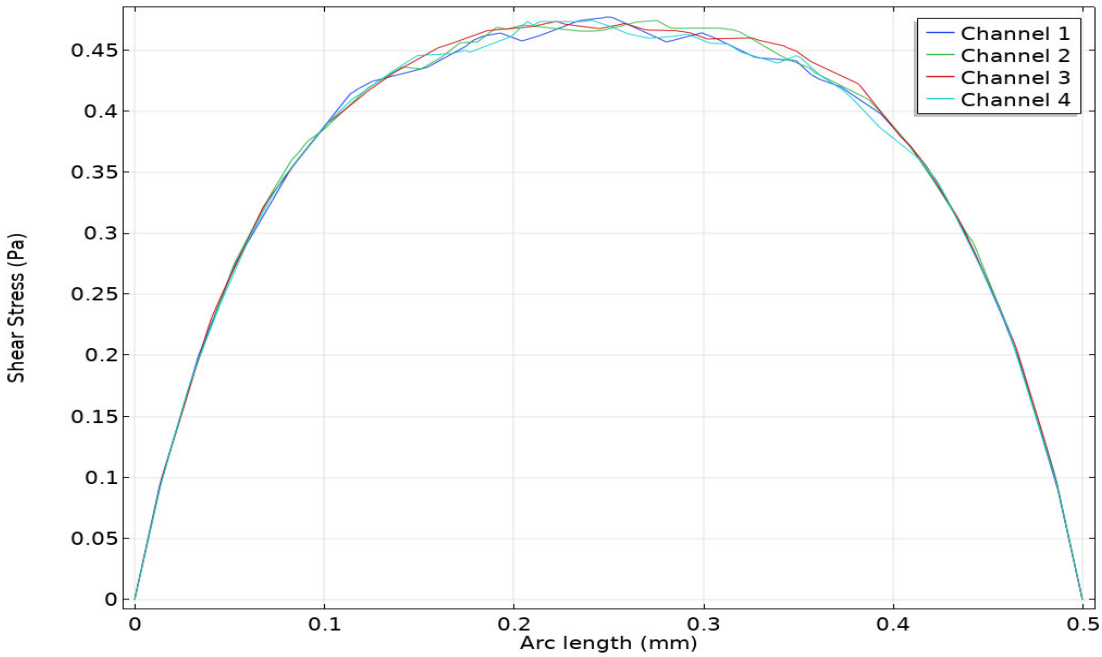

Maximum Shear Stress (Pa)				
Expected	**Channel 1**	**Channel 2**	**Channel 3**	**Channel 4**
0.5	0.4770	0.4743	0.4735	0.4743

Figure 29: **Shear Stress developed in each Channel:** *The shear stress developed along the width of the rectangular channels follows a parabolic distribution as expected. Since the flow rate in each channel is not completely equally distributed, the shear stress in each channel is different. The maximum shear stress in the channels is less than the desired 0.5Pa which is due to the flow velocities being less than the expected value. The desired shear stress can thus be obtained by applying a flow rate slightly higher than the calculated value.*

6.3) Conclusions

The flow simulation results of the proposed OoC design show that despite the distribution of flow in the four channels is less than the expected value, it is more or less equal. Channel 1 shows the highest achieved flow rate, achieving 49.8% of the flow rate applied at inlet while channel 3 achieves the least of 49.51%. When compared with adjacent channels, the differences in distribution is only 0.2% in case of channels 1 and 2 and only 0.07% in case of channels 3 and 4. The differences in flow rate although results in the generation of different maximum shear stress in each channel, the variations are very small with it being only 0.0035Pa higher in channel 1, where it is highest, than channel 3, where it is the least. The drop of flow rate below the desired value of 4.76µL/s causes it to be slightly below 0.5Pa which is desired for the endothelial cells to function properly like *in-vivo*.

6.4) Future Considerations

Due to device constraints, only a 'fine' mesh could be used. Producing a finer mesh may improve results and generate smoother plots. The mesh size may also be the

reason for the results obtained to be not symmetric which would be expected in the design. A reduction in the length of the section which leads the medium towards the branches can reduce the drop in the flow rate. Alteration of the height or width of the channel can also lead to better results. If the width of the channel is kept much greater than its height, then a flat flow profile shall be achieved and decreasing the height-by-width ratio can make the profile flatter than achieved in this case. A flatter profile will also lead to a more uniform shear stress distribution over the cell layer, along the channel width. However, despite a drop in the flow rate and reduction in the shear stress was achieved, the design showed almost uniform distribution of flow in the channel branches. To achieve 0.5Pa of shear stress, a flow rate higher than the calculated required flow rate may be applied.

APPENDIX – SUPPLEMENTARY FIGURES

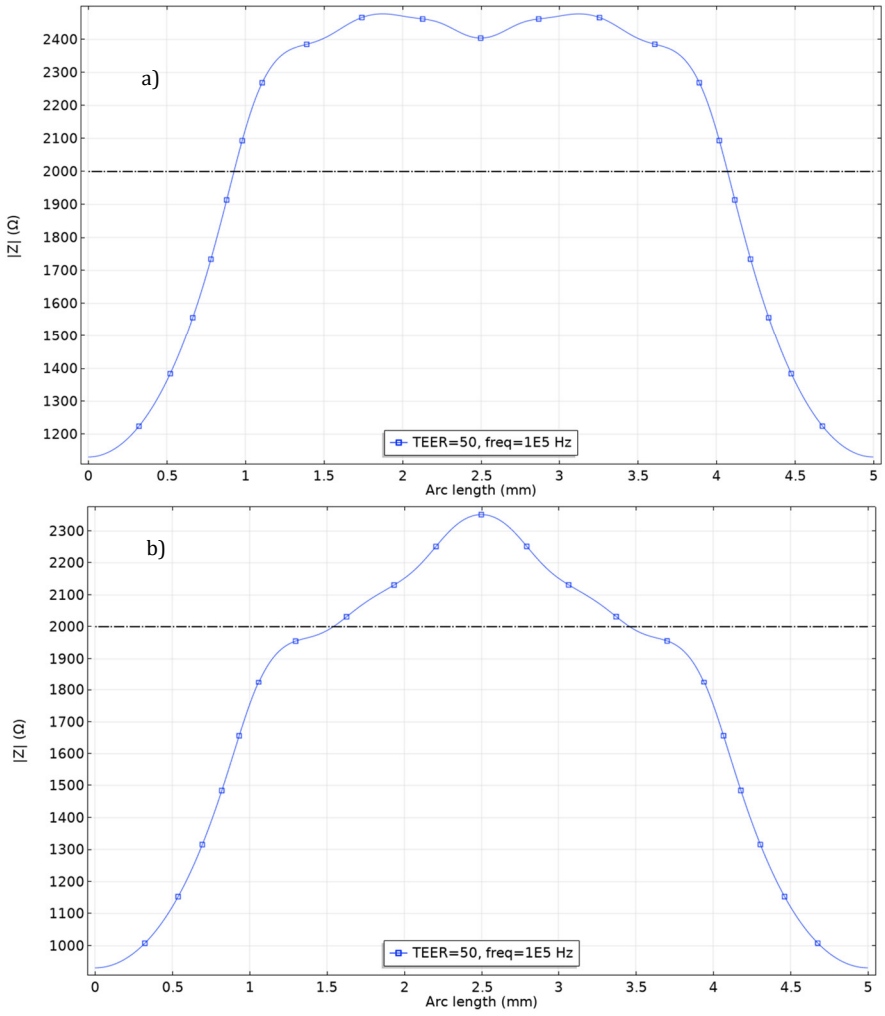

Figure A.1: **Measured Impedance magnitude along the length of the cell layer for 50Ω*cm² at 10000Hz:** *The figures show how the magnitude of the measurements depends on the sensitivity distribution. The impedance magnitude (here the resistance is measured) is obtained by multiplying the sensitivity with the conductivity of the cell layer. The measurements for configuration 1 is shown in (a) and that for configuration 2 is shown in (b). The dotted line indicates the actual value of the cell layer resistance for that particular TEER.*

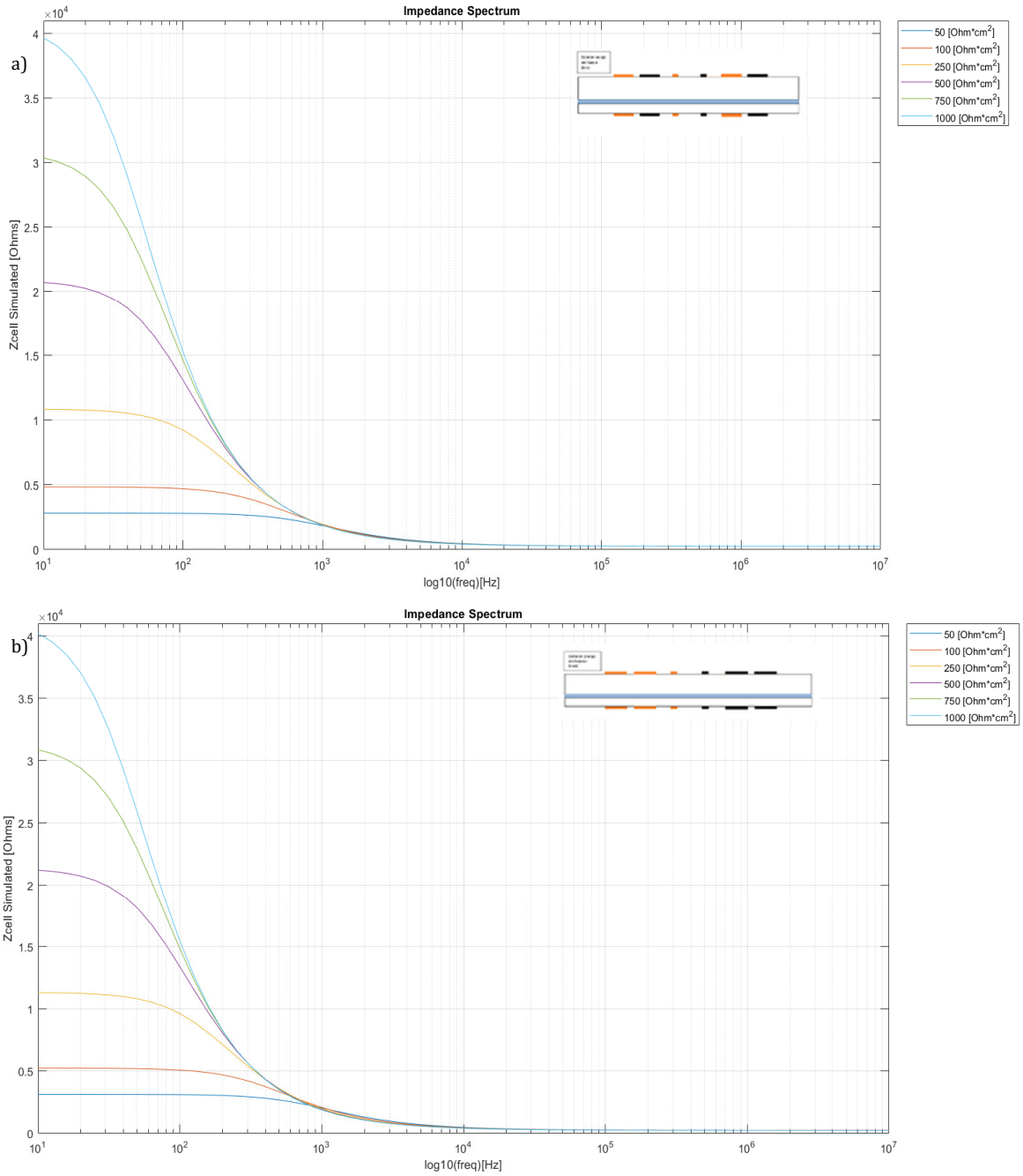

Figure A.2: **The Simulated Impedance Spectra for different TEER values:** *a) The semi-log impedance spectra obtained for configuration 1, b) the spectra obtained for configuration 2.*

REFERENCES

[1] Daneman R, Prat A (January 2015). "The blood-brain barrier". Cold Spring Harbor Perspectives in Biology. 7 (1): a020412.

[2] Dotiwala, Ary K., Cassidy McCausland, and Navdeep S. Samra. "Anatomy, Head and Neck, Blood Brain Barrier." StatPearls [Internet]. StatPearls Publishing, 2019.

[3] Obermeier, Birgit; Daneman, Richard; Ransohoff, Richard M. (2013). "Development, maintenance and disruption of the blood-brain barrier". Nature Medicine. 19 (12): 1584–1596.

[4] Pardridge, William M. "The blood-brain barrier and neurotherapeutics." NeuroRx 2.1 (2005): 1.

[5] Sweeney, Melanie D.; Sagare, Abhay P.; Zlokovic, Berislav V. (2018-01-29). "Blood–brain barrier breakdown in Alzheimer disease and other neurodegenerative disorders". Nature Reviews. Neurology. 14 (3): 133–150.

[6] Stamatovic, Svetlana M., Richard F. Keep, and Anuska V. Andjelkovic. "Brain endothelial cell-cell junctions: how to "open" the blood brain barrier." *Current neuropharmacology* 6.3 (2008): 179-192.

[7] Chen, Yan, and Lihong Liu. "Modern methods for delivery of drugs across the blood–brain barrier." *Advanced drug delivery reviews* 64.7 (2012): 640-665.

[8] Akhtar, Aysha. "The flaws and human harms of animal experimentation." Cambridge Quarterly of Healthcare Ethics 24.4 (2015): 407-419.

[9] Zhang, Boyang, et al. "Advances in organ-on-a-chip engineering." Nature Reviews Materials 3.8 (2018): 257-278.

[10] Bhatia, Sangeeta N., and Donald E. Ingber. "Microfluidic organs-on-chips." Nature biotechnology 32.8 (2014): 760-772.

[11] Rohr, Stephan, D. M. Schölly, and Andre G. Kleber. "Patterned growth of neonatal rat heart cells in culture. Morphological and electrophysiological characterization." Circulation research 68.1 (1991): 114-130.

[12] Whitesides, George M. "The origins and the future of microfluidics." Nature 442.7101 (2006): 368-373.

[13] Mahler, Gretchen J., et al. "Characterization of a gastrointestinal tract microscale cell culture analog used to predict drug toxicity." Biotechnology and bioengineering 104.1 (2009): 193-205.

[14] Borges, Nuno, et al. "Changes in brain microvessel endothelial cell monolayer permeability induced by adrenergic drugs." European Journal of Pharmacology: Molecular Pharmacology 269.2 (1994): 243-248.

[15] Hartz, Anika MS, David S. Miller, and Björn Bauer. "Restoring blood-brain barrier P-glycoprotein reduces brain amyloid-β in a mouse model of Alzheimer's disease." Molecular pharmacology 77.5 (2010): 715-723.

[16] Wang, Ying I., Hasan Erbil Abaci, and Michael L. Shuler. "Microfluidic blood–brain barrier model provides in vivo-like barrier properties for drug permeability screening." Biotechnology and bioengineering 114.1 (2017): 184-194.

[17] Bang, Seokyoung, et al. "A low permeability microfluidic blood-brain barrier platform with direct contact between perfusable vascular network and astrocytes." Scientific reports 7.1 (2017): 1-10.

[18] Yeon, Ju Hun, et al. "Reliable permeability assay system in a microfluidic device mimicking cerebral vasculatures." Biomedical microdevices 14.6 (2012): 1141-1148.

[19] Terrell-Hall, Tori B., et al. "Permeability across a novel microfluidic blood-tumor barrier model." Fluids and Barriers of the CNS 14.1 (2017): 1-10.

[20] Booth, Ross, and Hanseup Kim. "Characterization of a microfluidic in vitro model of the blood-brain barrier (μBBB)." Lab on a Chip 12.10 (2012): 1784-1792.

[21] Griep, Lonneke M., et al. "BBB on chip: microfluidic platform to mechanically and biochemically modulate blood-brain barrier function." Biomedical microdevices 15.1 (2013): 145-150.

[22] van der Helm, Marieke Willemijn. "Electrical and microfluidic technologies for organs-on-chips: Mimicking blood-brain barrier and gut tissues." (2018).

[23] Henry, Olivier YF, et al. "Organs-on-chips with integrated electrodes for trans-epithelial electrical resistance (TEER) measurements of human epithelial barrier function." Lab on a Chip 17.13 (2017): 2264-2271.

[24] Maoz, Ben M., et al. "A linked organ-on-chip model of the human neurovascular unit reveals the metabolic coupling of endothelial and neuronal cells." Nature biotechnology 36.9 (2018): 865-874.

[25] Elbrecht, Daniel H., Christopher J. Long, and James J. Hickman. "Transepithelial/endothelial Electrical Resistance (TEER) theory and applications for microfluidic body-on-a-chip devices." tc 1.1 (2016): 1.

[26] Yeste, J., et al. "A novel strategy to monitor microfluidic in-vitro blood-brain barrier models using impedance spectroscopy." Bio-MEMS and Medical Microdevices II. Vol. 9518. International Society for Optics and Photonics, 2015.

[27] Yeste, J., et al. "Geometric correction factor for transepithelial electrical resistance measurements in transwell and microfluidic cell cultures." Journal of Physics D: Applied Physics 49.37 (2016): 375401.

[28] Zakharova, M., et al. "Multiplexed blood–brain barrier organ-on-chip." Lab on a Chip 20.17 (2020): 3132-3143.

[29] Park, DoYeun, et al. "Integrating organs-on-chips: multiplexing, scaling, vascularization, and innervation." Trends in biotechnology 38.1 (2020): 99-112.

[30] Srinivasan, Balaji, et al. "TEER measurement techniques for in vitro barrier model systems." Journal of laboratory automation 20.2 (2015): 107-126.

[31] Haorah, James, et al. "Activation of protein tyrosine kinases and matrix metalloproteinases causes blood-brain barrier injury: Novel mechanism for neurodegeneration associated with alcohol abuse." Glia 56.1 (2008): 78-88.

[32] Benson, Kathrin, Sandra Cramer, and Hans-Joachim Galla. "Impedance-based cell monitoring: barrier properties and beyond." Fluids and Barriers of the CNS 10.1 (2013): 1-11.

[33] Singh Y. Electrical Resistivity Measurements: A Review. Int J Mod Phys Conf Series. 2013; 22: 745-756

[34] World Precision Instruments evom2 manual. http://https://www.wpi-europe.com/products/cell-and-tissue/teer-measurement/evom2.aspx.

[35] Heaney, Michael B. "Electrical conductivity and resistivity." The measurement, instrumentation and sensors handbook (2000): 1332-1345.

[36] Gray, P.R.; Hurst, P.J.; Lewis, S.H.; Meyer, R.G. (2001). Analysis and Design of Analog Integrated Circuits (4th ed.). New York: Wiley. ISBN 0-471-32168-0.

[37] Grimnes, Sverre, and Orjan G. Martinsen. Bioimpedance and bioelectricity basics. Academic press, 2011.

[38] Goedbloed, Jasper J. "Reciprocity and EMC measurements." *TIJDSCHRIFT-NERG* 71.1 (2006): 15.

[39] Pettersen, Fred J. "On sensitivity in transfer impedance measurements." Journal of Electrical Bioimpedance 9.1 (2018): 159-162.

[40] Kauppinen, P., Hyttinen, J. & Malmivuo, J. (2006). Sensitivity distribution visualizations of impedance tomography measurement strategies. International Journal of Bioelectromagnetism, 8(1): 1-9.

[41] Grimnes, S., & Martinsen, Ø. G. (2006). Sources of error in tetrapolar impedance measurements on biomaterials and other ionic conductors. Journal of Physics D: Applied Physics, 40(1), 9.

[42] Nicander, I., et al. "Electrical impedance measured to five skin depths in mild irritant dermatitis induced by sodium lauryl sulphate." British Journal of Dermatology 132.5 (1995): 718-724.

[43] Odijk, M., Van der Meer, A.D., Levner, D., Kim, H.J., Van der Helm, M.W., Segerink, L.I., et al. (2015). Measuring direct current trans-epithelial electrical resistance in organ-on-a-chip microsystems. Lab on a Chip, 15(3): 745-752.

[44] Leffers, L., Ebert, F., Taleshi, M.S., Francesconi, K.A. & Schwerdtle, T. (2013). In vitro toxicological characterization of two arsenosugars and their metabolites. Molecular Nutrition & Food Research, 57(7): 1270-1282.

[45] Bard, A.J. & Faulkner, L.R. (2001). Electrochemical methods: fundamentals and applications. J. Wiley & Sons.

[46] Farsaci, Francesco, et al. "On evaluation of electric conductivity by mean of non-equilibrium thermodynamic approach with internal variables. An application to human erythrocyte suspension for metabolic characterizations." Journal of Molecular Liquids 224 (2016): 1181-1188.

[47] Dean DA, Ramanathan T, Machado D, Sundararajan R. Electrical Impedance Spectroscopy Study of Biological Tissues. J Electrostat. 2008;66(3-4):165-177. doi: 10.1016/j.elstat.2007.11.005

[48] Kaiser, Kenneth L. Electromagnetic shielding. Crc Press, 2005.

[49] Szydzik, C., et al. "Fabrication of complex PDMS microfluidic structures and embedded functional substrates by one-step injection moulding." *RSC advances* 6.91 (2016): 87988-87994.

[50] Ceyssens F., Puers R. (2012) SU-8 Photoresist. In: Bhushan B. (eds) Encyclopedia of Nanotechnology. Springer, Dordrecht. https://doi.org/10.1007/978-90-481-9751-4_360

[51] H. N. Chan, Y. Chen, Y. Shu, Y. Chen, Q. Tian and H. Wu, Microfluidics and Nanofluidics, 2015, 19, 9-18

[52] Wong, A.D., Ye, M., Levy, A.F., Rothstein, J.D., Bergles, D.E. & Searson, P.C. (2013). The blood-brain barrier: an engineering perspective. Frontiers in Neuroengineering, 6: 7

[53] Son, Y. (2007). Determination of shear viscosity and shear rate from pressure drop and flow rate relationship in a rectangular channel. Polymer, 48(2): 632-637.